Three-Dimensional Image Reconstruction of Insect Flight Muscle. II. The Rigor Actin Layer

K. A. Taylor, M. C. Reedy, L. Córdova, and M. K. Reedy

The Department of Cell Biology, Duke University Medical Center, Durham, North Carolina 27710

Abstract. The averaged structure of rigor cross-bridges in insect flight muscle is further revealed by three-dimensional reconstruction from 25-nm sections containing a single layer of thin filaments. These exhibit two thin filament orientations that differ by 60° from each other and from myac layer filaments. Data from multiple tilt views (to ±60°) was supplemented by data from thick sections (equivalent to 90° tilts). In combination with the reconstruction from the myac layer (Taylor et al., 1989), the entire unit cell is reconstructed, giving the most complete view of in situ cross-bridges yet obtained. All our reconstructions show two classes of averaged rigor cross-bridges. Lead bridges have a triangular shape with leading edge angled at ~45° and trailing edge angled at ~90° to the filament axis. We propose that the lead bridge contains two myosin heads of differing conformation bound along one strand of F-actin. The lead bridge is associated with a region of the thin filament that is apparently untwisted. We suggest that the untwisting may reflect the distribution of strain between myosin and actin resulting from two-headed, single filament binding in the lead bridge. Rear bridges are oriented at ~90° to the filament axis, and are smaller and more cylindrical, suggesting that they consist of single myosin heads. The rear bridge is associated with a region of apparently normal thin filament twist. We propose that differing myosin head angles and conformations consistently observed in rigor embody different stages of the power stroke which have been trapped by a temporal sequence of rigor cross-bridge formation under the constraints of the intact filament lattice.

CROSS-BRIDGE structure in the absence of ATP is believed to reflect the conformational state of myosin heads at the end of the power stroke of ATP-driven contraction. The force-generating event has long been thought to involve changes in the angle of attachment between actin and myosin (Reedy et al., 1965; Huxley, 1969). Two attractive candidates for these different angles include one at 90° to the filament axis, representing the beginning of the power stroke, and another at 45° orientation representing the end of the cycle.

The 90° orientation hypothesized for the beginning of the power stroke has proved difficult to characterize. It is an extrapolation from the 90° orientation of myosin heads observed in ATP-relaxed muscle (Reedy et al., 1965), which are not attached to actin. Several attempts to trap this state using preparations of the complex between F actin and myosin subfragment-1-([S1]¹acto-S1) have not observed a unique orientation (Craig et al., 1985; Applegate and Flicker, 1987). Only recently have coordinated mechanical and structural experiments on fibers succeeded in trapping and characterizing nucleotide-bearing cross-bridges attached to actin at a 90° angle (Reedy et al., 1988*a*,*b*).

The 45° state observed in rigor muscle is held to be equivalent to the structure at the end of the power stroke. Rigor is an attractive candidate for the end of the power stroke because the angle of rigor chevrons is in the appropriate direction to bring about filament sliding and sarcomere shortening. The 45° angle has been inextricably tied to the rigor state, to the extent that the "45° state" and "rigor state" are used interchangeably. This is understandable because angled heads with an overall tilt of ~45° have been described repeatedly in original images (Reedy et al., 1965; Reedy and Reedy, 1985) and three dimensional (3-D) reconstructions of acto-S1 (Moore et al., 1970; Taylor and Amos, 1981; Vibert and Craig, 1982; Toyoshima and Wakabayashi, 1985; Milligan and Flicker, 1987). This view of rigor cross-bridges with a uniform structure has been supported by x-ray diffraction patterns of rigor insect (fibrillar) flight muscle (IFM) which can be reasonably modeled with a single shape and angle for the myosin heads (Miller and Tregear, 1972; Rodger and Tregear, 1974; Holmes et al., 1980). That a cross-bridge conformation similar to rigor occurs during contraction is consistent with electron paramagnetic resonance measurements which have indicated that in rigor the probe has a narrowly defined orientation (Barnett and Thomas, 1984; Thomas and Cooke, 1980; Thomas et al., 1983), and that up to 20% of the signal in electron paramagnetic resonance spectra of contracting muscle arises from probes with this

1. *Abbreviations used in this paper*: acto-S1, complex between F actin and S1; AMPPNP, adenosine 5'-[β,λ-imido]triphosphate; HMM, heavy meromyosin; IFM, insect (fibrillar) flight muscle; S1, myosin subfragment-1; 3-D, three-dimensional.

narrow rigor-like orientation (Cooke et al., 1982). In addition, fluorescent probes at the nucleotide site do not change from the rigor orientation during muscle contraction (Yanagida, 1984, 1985).

However, many observations appear inconsistent with a model in which force is produced by the rotation of the whole myosin head from a 90° to a 45° angle. Time resolved x-ray diffraction has not found evidence for rigor-like cross-bridges even transiently during isometric contraction (Matsubara et al., 1984; Maeda et al., 1986; Wakabayashi et al., 1988). Correlative electron microscopy and mechanical studies of *Lethocerus* fibers in the presence of adenosine 5'-[β,λ-imido]triphosphate (AMPPNP) have shown a large tension loss without an apparent change in tilt angle and without a coincident drop in rigor stiffness (Reedy et al., 1988*a*,*b*). In contrast to the club-shaped structure commonly used to describe myosin heads, a recent interpretation of 3-D reconstructions of acto-S1 has suggested that the myosin head consists of domains that are oriented at different angles to the filament axis in rigor (Toyoshima and Wakabayashi, 1985). In modeling x-ray diagrams of rigor IFM, the optimal angle is actually nearer to 90° than the 45° angle widely assigned to rigor cross-bridges in situ and considerably greater than the tilt angle of some domains observed in acto-S1. Moreover, the interpretation of the spectroscopic data is equally compatible with a model in which one part of the myosin head maintains a constant conformation close to actin in all attached states, while other parts of the head move or realign in different states (Goody and Holmes, 1983).

Based on our electron microscopy and 3-D reconstructions of IFM we have shown that rigor structure encompasses two forms of cross-bridges that differ in tilt angle, size, density, and slew. Furthermore, we suggest that one of the two bridge classes consists of two myosin heads of different conformation. Here we examine a 3-D reconstruction of a rigor actin layer obtained from multiple tilt views combined with orthogonal projections obtained from thick sections. The importance of the actin layer lies in the fact that it contains two thin filaments that differ in orientation by 60° from the single filament observed in the myac layer. In combination with the myac layer, it reconstructs the complete hexagonal unit cell. This 3-D reconstruction represents an extended test of the validity of the two classes of rigor cross-bridges and confirms the findings of our previous studies. Our results suggest that rigor cross-bridge conformation in situ is more complex than previously thought and suggests that these different rigor structures may have important implications for understanding force generation during muscle contraction.

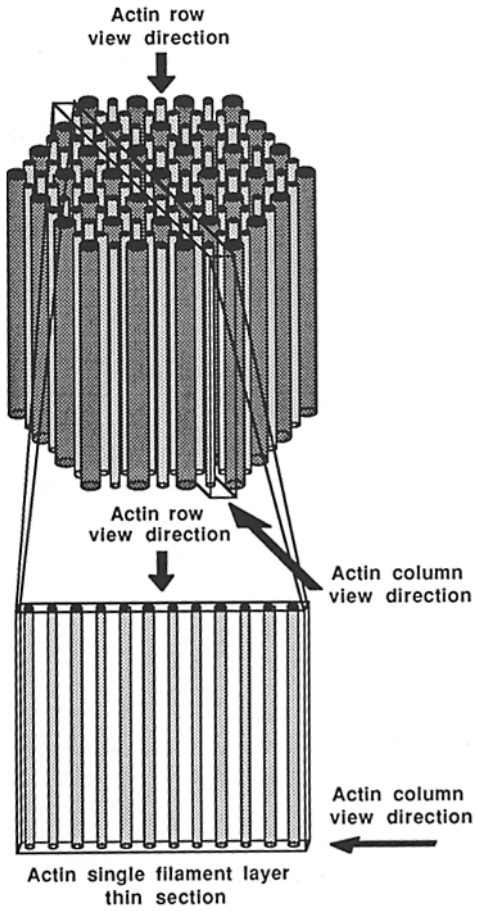

Figure 1. Diagram illustrating the relationship between the views of the actin layer derived from thick sections to the actin layer itself. Actin layers occur in 20–25-nm-thick longitudinal sections cut parallel to the 10.0 planes of the hexagonal filament lattice. These actin layers contain only thin filaments with the thick filament features cut away by the sectioning process. The sectioning process is physically akin to windowing from the 3-D filament lattice. "Actin rows" are rows of thin filaments windowed out of images of thick transverse sections viewed down the 00.1 direction and are equivalent in view direction to actin layers tilted 90° about an axis perpendicular to the filament axis. Their Fourier transform provides a complete equatorial plane of the actin layer transform. "Actin columns" are thin filaments windowed out of images of thick longitudinal sections viewed down the 10.0 planes and are equivalent in view direction to actin layers tilted 90° about an axis parallel to the filament axis. Their Fourier transform provides a complete meridional plane of the actin layer transform.

Materials and Methods

Specimen Preparation and Electron Microscopy

Specimen preparation and electron microscopy were carried out as described previously for the rigor myac layer (Taylor et al., 1984*b*, 1989). Two tilt series to ±60° in 10° steps were supplemented by ±60° tilts taken with tilt axes at angles of 37°, 71°, and 150° to the *a* axis of the unit cell (Table I).

Image Analysis and Reconstruction Protocol

The 3-D reconstruction was done with the same methods as the rigor myac layer described previously (Taylor et al., 1984*b*, 1986, 1989) by combining merged tilt series data with projection data obtained from a thick transverse and a thick longitudinal section. This reconstruction scheme, illustrated in Fig. 1, provides three mutually orthogonal views of the actin layer in addition to those views provided by the tilted thin section. The microtomy process in effect "windows" the actin layer from the 3-D filament lattice. Views orthogonal to the plane of the actin layer are obtained from appropriately windowed areas of the thick section images.

Tilt series electron micrographs were digitized at a step size of 1.76 nm on a densitometer constructed in this laboratory by W. Longley and D. A. Kopf (Taylor et al., 1984*a*) and the actin row and actin column data digitized as described (Taylor et al., 1989). The transforms were sampled on an axial 116-nm period, the smallest period that contains integral multiples of the 14.5-nm-thick filament period and the 38.7-nm-thin filament period. The phase origin refinement and merging steps were carried out in the two-sided plane groups p1, in which no symmetry elements are present and p12 (nomenclature of Holser [1958]), in which a pair of twofold rotation axes are presumed to be present running coincident with the two filament axes. The quality of fit was similar in both cases, although slightly better when

Table I. Image Data Summary

Image	Tilt axis	Tilt angle	p1 phase residual	p2 phase residual
407	0.2	0.0	7.2	10.3
408	0.2	−62.3	11.9	14.9
409	0.2	50.0	11.5	18.0
410	0.2	45.2	9.7	15.1
411	0.2	−52.6	8.8	11.5
412	0.2	−42.4	11.1	12.3
413	0.2	34.8	12.2	20.6
414	0.2	26.9	11.4	17.7
415	0.2	−31.5	11.5	10.1
417	0.2	−23.5	7.3	15.7
418	0.2	13.5	9.6	16.5
419	0.2	10.1	8.6	12.3
420	0.2	−11.9	8.5	11.0
421	150.7	62.4	9.5	11.6
422	150.7	54.7	13.0	21.9
423	95.7	59.5	10.8	23.2
424	95.7	−59.8	8.6	13.4
425	95.7	−49.1	9.4	14.3
426	95.7	48.9	13.9	16.6
427	95.7	39.9	10.8	14.8
428	95.7	−40.5	10.0	14.6
429	95.7	−29.4	7.0	10.9
430	95.7	29.4	9.3	9.2
431	95.7	18.5	9.0	13.4
432	95.7	−21.0	9.2	12.9
433	95.7	−11.1	7.4	7.6
434	95.7	5.6	10.2	12.9
435	71.7	53.3	12.7	15.7
436	71.7	−61.2	7.0	12.8
437	37.0	61.5	9.0	17.1
438	37.0	−52.0	10.3	12.6
439	95.7	0.0	8.5	7.8

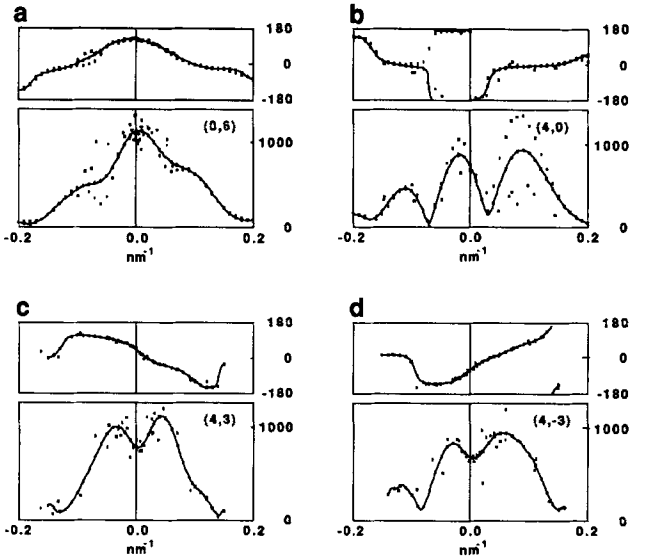

Figure 2. Selected lattice lines used in the reconstruction. Upper diagram shows phases (degrees), lower diagram amplitude (arbitrary units). (*a*) Meridional (0,6) at an axial spacing of 19.33 nm. (*b*) Equatorial (4,0) lattice line at a spacing of 11.66 nm. *c* and *d* are symmetry-related off-meridional lattice lines at a spacing of 11.16 nm. For perfect twofold rotational symmetry about the meridional axis, the phase profile of *d* is related to that of *c* by the relationship: phase (4,3,Z*) = −phase (4,−3,Z*).

no symmetry is assumed, i.e., in p1 (Table I). Transform data not falling on orders of the 38.7-nm axial period was weak (it is generally not observed in optical diffraction patterns) and correlated poorly among all the images analyzed. The single exception was the data on the 14.5-nm layer line, which although weak, was reproducible within the tilt series data for images which sampled the same region of the lattice line.

In addition to the (0,0) lattice line, six equatorial lattice lines were obtained from the actin row images and nine meridional lattice lines were obtained from the actin columns. Five actin rows and seven actin columns were used to calculate averaged data sets for addition to the tilt series data. Among the seven actin column data sets, there was good agreement for only the lattice lines falling on the 0, 3rd, 6th, 8th, and 9th orders of the 116.0-nm meridional period. Lattice line data from the thick sections correlated poorly at Z^* resolutions exceeding 0.2 nm^{-1}. The quality of fit as measured by the phase residuals relative to their respective average was 26° for the actin row data (range 20°-31°) and 40° for the actin column data (range 30°-47°).

The alignment of data from the thick sections with tilt series data was done by cross-correlation of the averaged actin row with lattice lines fitted to the merged equatorial tilt series data and by cross-correlation of actin column data with lattice lines fitted to the merged meridional tilt series data. The actin row data had to be stretched by a factor of 1.7 along Z^* (the transform direction normal to the section plane) to obtain acceptable phase residuals. This alignment, which was tested over all four possible relative orientations, yielded an amplitude weighted phase residual of 36.7°. The best agreement between the two data sets was observed for the even ordered lattice lines and the (1,0), and somewhat less for the (3,0) and (5,0) lattice lines. A similar procedure was carried out for just the 3rd, 6th, 8th, and 9th orders of the 116-nm period of the actin column data with result that the best Z^* scaling factor was 1.8 and the phase residual was 26.4°. The overall agreement between the actin row and the actin column data with the tilt series data was better with respect to phases than with respect to amplitudes (Fig. 2). Smooth curves were fit to the combined lattice line data by a least squares procedure that assumed a section thickness of 25 nm. There was near mirror symmetry of amplitude and phase profiles for the meridional data (e.g., the [0,6] lattice line) and the close approximation with real phases for the equatorial data (e.g., the [4,0] lattice line) as shown in Fig. 2.

The in-plane resolution obtained for the reconstruction was somewhat less than that obtained in the myac layer reconstruction (Taylor et al., 1984*b*, 1989). While this could indicate less order in the actin layer, it is more likely due to a difference in the molecular transform of the actin layer, which does not include thick filaments. The intrinsic order of myac and actin layers, which come from the same filament lattice, are not independent quantities. Nevertheless, optical diffraction patterns of actin layers rarely show spots beyond the 6th equatorial order, while those from myac layers nearly always diffract to eight equatorial orders. Therefore, the high equatorial resolution of myac layers manifests the effect of the thick filaments on the molecular transform, and is not due to higher intrinsic order. The final data set contains structure factors extending to a resolution of ~5 nm in Z^* while the resolution within the plane is 7.7 nm in the equatorial direction and 12.9 nm in the axial direction.

Rotational correlation analyses were determined by calculating the correlation coefficient according to the formula described previously (Taylor et al., 1989). Maps of thin filaments in the actin layer were calculated from structure factor data having the phase origin on the presumptive twofold rotation axis, therefore obviating any requirement to determine the translational alignment.

Acto-S1 helical projections were also used in rotational cross-correlations with thin filaments windowed from the actin layer reconstruction. These helical projections were calculated from previously published layer line data (Taylor and Amos, 1981). These maps had their contrast reversed to match that of the images of the positively stained actin layer. The sensitivity of the rotational cross-correlations to the motif shape was assessed using acto-S1 helical projection maps calculated with different sets of layer lines. These variations included maps that had been calculated both with and without equators and with and without 4th and 6th layer lines. The thin filament images from the actin layer were windowed from reconstructions that had been corrected for various amounts of mass loss by expanding the map in a direction perpendicular to the section plane.

Surface images of the reconstruction were calculated using a program written by Dr. Guy Vigers (Vigers et al., 1986) and displayed on a LEX-90 (Lexidata Corp., Billerica, MA). All surface images were calculated from

3-D maps stretched in the Z direction by a factor of 1.8 to compensate for section thinning.

Tilt Angle and Viewing Conventions

The tilt angle convention used here is as described in Fig. 1 of Reedy and Reedy (1985). Longitudinal views of the reconstructions are always oriented with the Z line at the bottom, M line at the top. Transverse views of the reconstruction are always viewed towards the Z line. Z and Z^* denote the real and reciprocal space directions perpendicular to the actin layer plane.

Results

Actin Layer Morphology and Diffraction

Actin layers occur in regions of 20–25-nm longitudinal sections from which the thick filaments have been excluded, leaving only thin filaments within the section. In actin layers these thin filaments alternate between two orientations that differ by 60° from one another and from the single filament orientation in the myac layer. The 38.7-nm period is marked on thin filaments by a doublet comprising two classes of cross-bridges which we designate as lead and rear according to their positions in double chevrons of myac layers. In this discussion we will use the symbols Z and N as icons (Fig. 3) to distinguish the two thin filament orientations in the actin layer (Reedy and Reedy, 1985).

Rigor actin layers in untilted projections are characterized by a cross-bridge pattern of alternating dense beads and transverse strips which mark an axial repeat of 38.7 nm along thin filaments (Fig. 3). The dense beads are staggered by ~12.9 nm on adjacent thin filaments and are due to projections of cross-bridge mass extending approximately normal to the section plane. Reedy and Reedy (1985) showed that on Z filaments, these beads are projections of lead bridges and on N filaments, of rear bridges. The transverse strips are formed by in-register "ladder rungs". Each rung was shown to arise from one lead and one rear bridge diverging from a common or near-common origin on the adjacent excluded thick filament.

The actin layer selected for 3-D reconstruction appeared homogeneous over nearly a half sarcomere (Fig. 3). Its diffraction pattern consists of the equatorial and three non-equatorial layer lines that are orders of the 38.7-nm actin period. These layer lines have near mirror symmetry about the meridional (filament) axis thus indicating that the filament layer is well-centered within the section. A weak 14.5-nm meridional spot is always present in rigor actin layers in spite of the exclusion of thick filaments from which this period is known to arise. Haselgrove and Reedy (1978) have suggested that a 14.5-nm period on the thin filaments in rigor arises from an average separation of 14.5 nm between attached cross-bridges, expressing the influence of the original thick filament repeat on selection of sites along the actin subunit repeat. The beating between the 14.5-nm-thick filament and 38.7-nm-thin filament periods gives the cross-bridge lattice a long 116-nm axial period.

We supplemented the data from tilt series with data derived from thick transverse and thick longitudinal sections (Fig. 1). This procedure provides transform data within a "missing cone" that is defined by physical restrictions on specimen tilt angle in the microscope. These additional data consist of complete equatorial and meridional planes of the 3-D actin layer transform. The thick section images selected had regions with near-circular thick filament profiles (transverse section) and as little sarcomere "barrel shape" as possible (longitudinal section). The same micrographs were used for these as for the myac layer (Taylor et al., 1989), here windowed differently in keeping with the actin layer thin section geometry. In the actin columns (Fig. 4 *b*) the filaments have density repeating on a 38.7-nm period but do not show prominent 19.3- and 12.9-nm periods. Typically, the actin column diffraction (Fig. 4 *b*) is dominated by the equatorial (0,0) lattice line. The meridional lattice lines of the 116-nm period are much weaker and decrease in intensity in the order (0,3), (0,6), (0,9), (0,8). In the actin rows the thin filament profile is predominantly oval (Fig. 4 *a*). The axial projection profiles of the pair of thin filaments that make up the repeating unit have their corresponding features oriented at ±60° to the plane of the actin layer. This rotation gives rise to the near extinction of the (1,0) diffraction spot in transforms of untilted actin layers and the distinct splitting of the (1,0) lattice line into a corresponding pair of intense peaks. Typically, actin row diffraction (Fig. 4 *a*) has strong even ordered and weak odd ordered lattice lines with the exception of the previously mentioned (1,0).

Features of the Actin Layer Reconstruction

The reconstructed actin layer is ~10-nm thick, or only about half the predicted thickness based upon the known filament geometry and lattice dimensions of insect flight muscle. This thickness, however, is consistent with expectations based on the amount of Z^* scaling that was required to fit the thick section lattice line data with the merged tilt series data. The low thickness value presumably results from electron irradiation-induced mass loss from the section (Bennett, 1974; Berriman and Leonard, 1986). This section thinning has been compensated where indicated by stretching the reconstruction by a factor of 1.8 in the direction normal to the section plane.

The reconstruction also has a high degree of twofold symmetry about the two filament axes as judged by both the low phase residuals in p12 and by the minimal differences in the p1 (Fig. 5 *a*) and p12 reconstructions (Fig. 5 *b*). Enforcing twofold symmetry smears out the rear bridge density axially along the thin filament long-pitch helices. In addition, some low density features, which are probably noise, seen on only

Figure 3. Electron micrograph of the untilted rigor actin layer, with the area used for the reconstruction outlined. Cross-bridges are seen here as triangularly shaped profiles which flare out at their bases to form "ladder rungs" between filaments marking the 38.7-nm repeat. The optical diffraction pattern is shown in the top inset. The 3rd, 6th, and 9th meridional orders occur at spacings of 1/38.7, 1/19.3, and 1/12.9 nm^{-1}. The two filaments are identified by the icons Z and N, as shown in the lower inset, according to the convention adopted by Reedy and Reedy (1985). In this nomenclature, the orientation of the diagonal center bar of N and Z represents the direction of the line connecting each thin filament with the two out-of-section-plane thick filaments from which it receives cross-bridges. This center bar makes an angle of −60° (\ direction) or +60° (/ direction) to the section plane. The underline in N or Z indicates the front surface of the section.

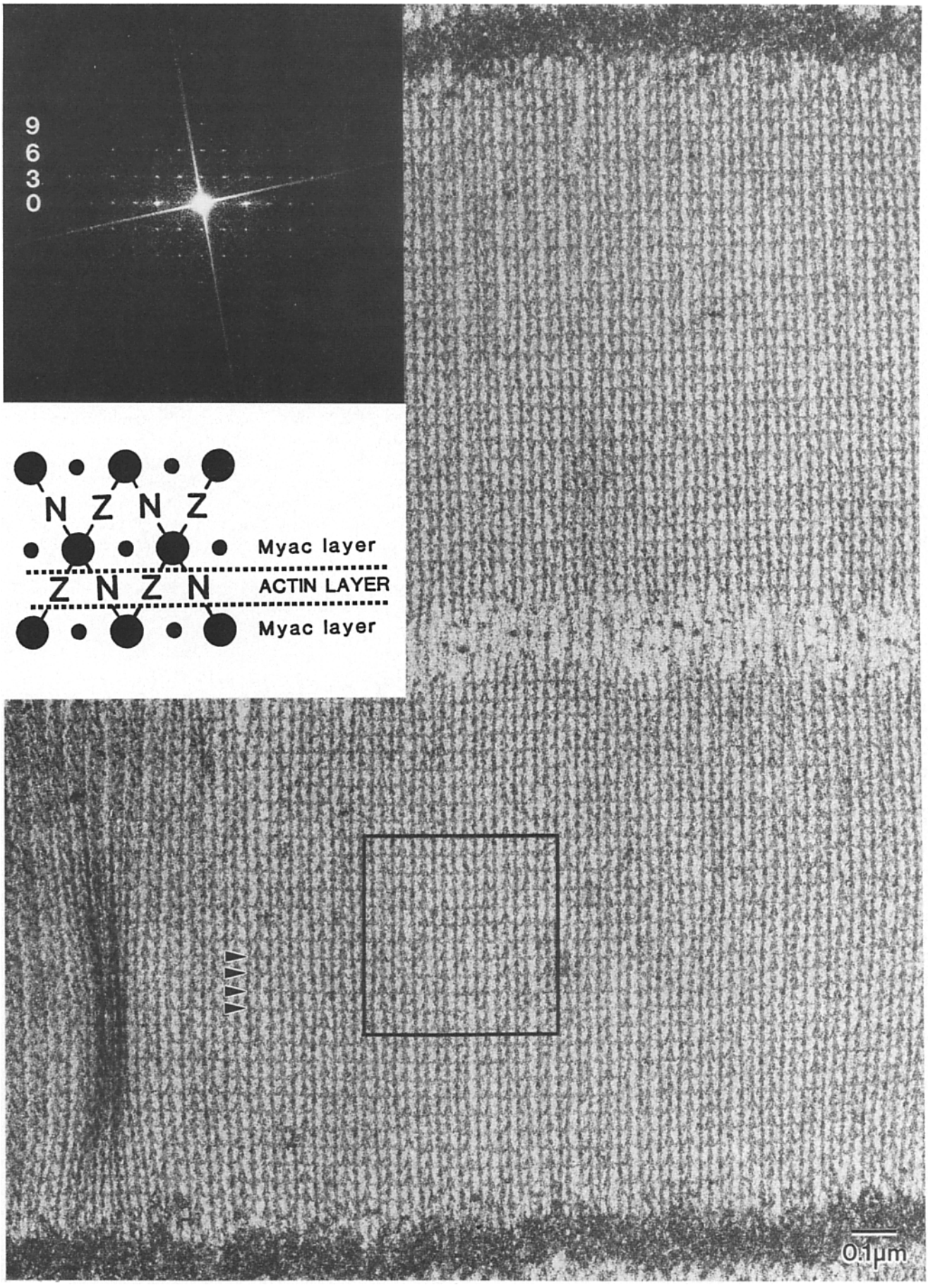
9
6
3
0
N Z N Z
Myac layer
Z N Z N
ACTIN LAYER
Myac layer
0.1μm

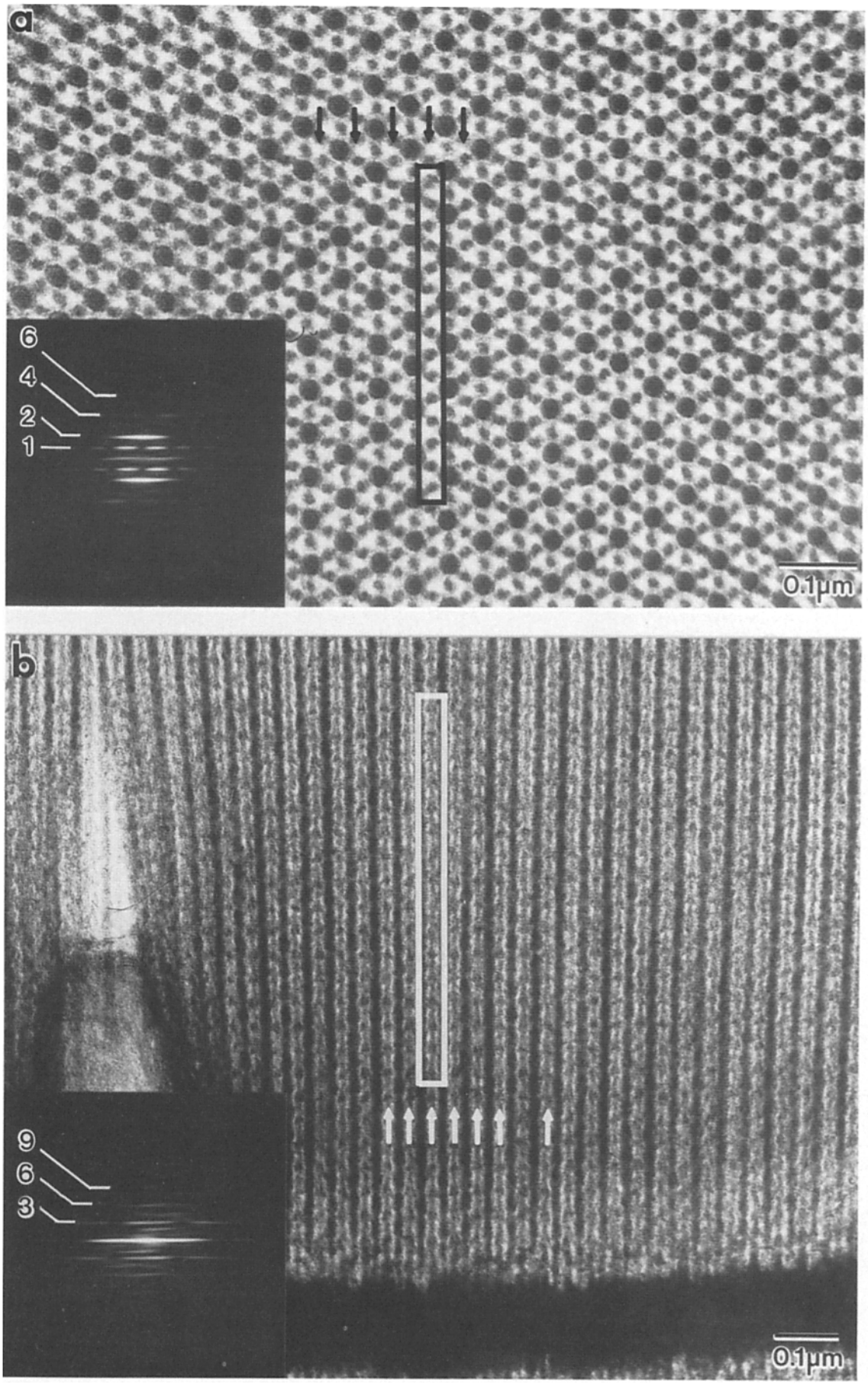
a
6
4
2
1
0.1μm
b
9
6
3
0.1μm

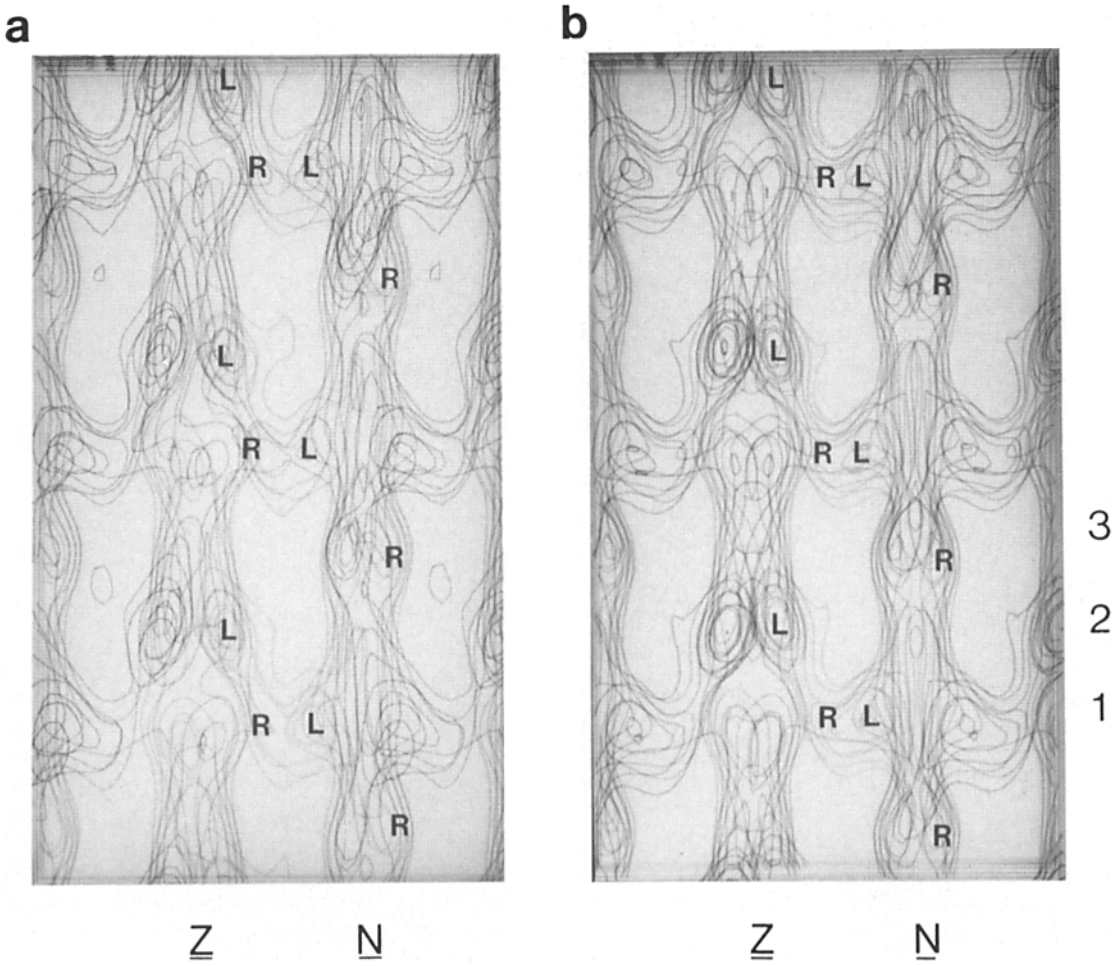

Figure 5. Three-dimensional contour maps of rigor IFM actin layer. The selection of contour cutoff for display was made such that the rear bridges could be clearly visualized. This requires a low contour level which also enlarges the dimensions of other components in the 3-D reconstruction. (*a*) Map of the reconstruction done in the two-sided plane group p1 and (*b*) as obtained when the reconstruction is done in two-sided plane group p12. In this orientation a thick filament would be positioned in the center of the map at the back between the Z and N thin filaments. A pair of thick filaments would be positioned at the front, one to the left of the Z filament and one to the right of the N filament. Lead and rear bridges are labeled L and R, respectively. The pattern of cross-bridges at the back of the reconstruction, labeled diagonally (\) R-L-R-L from N filament to Z filament, describes a left-handed helix about the axis of the thick filament. This is the helix of actin targets (Reedy, 1968) that surrounds each thick filament. On the thin filament each actin target consists of a lead bridge subtarget and a rear bridge subtarget. The axial 116-nm repeat, which runs vertically in the figure, contains three pairs of lead and rear bridges per actin filament.

one side of the section plane in the p1 reconstruction (Fig. 5 *a*), are lost when twofold symmetry is enforced (Fig. 5 *b*).

Many cross-bridge features observed in the three different views presented by actin and myac layers are remarkably constant. One feature common to both lead and rear bridges is their sigmoidal shape seen in cross-sectional views (see Fig. 7). It is convenient to describe this sigmoid in terms of two components. The opposed cross-bridge pairs of each chevron form a midsegment, oblong in cross section, composed of the actin-binding domains of the myosin heads merged with the intervening thin filament density, and also form a neck-stem component at each end of the midsegment connecting it to the thick filaments. The neck-stem extends tangentially from the midsegment to define the clockwise or anticlockwise slew of the complex. We consider neck-stems as consisting of neck and stem domains (Reedy and Reedy, 1985). The stem is identified with the back-bent portion of the cross-bridge seen in micrographs of flared-X layers (Reedy and Reedy, 1985) and in myac layer 3-D reconstructions (Taylor et al., 1984*b*, 1989), connecting the bridge

Figure 4. Electron micrographs of the thick sections of rigor IFM used in the reconstruction. These fibers are from the same bundle used for the actin layer. (*a*) Thick transverse section with an actin row outlined. Arrows indicate the positions of other actin rows used in the averaged data. (*b*) Thick longitudinal section with an actin column outlined. Arrows indicate positions of other actin columns used in the averaged data. Computed diffraction patterns of the windowed regions are shown in the insets. The amplitude profiles of the equatorial layer lines (shown in *a*) and the meridional layer lines (shown in *b*) provide similar information to that given by the amplitude portion of the lattice line plots shown in Fig. 2.

neck with the thick filament. In actin layer 3-D reconstructions, the stem is not readily visualized because on half of the bridges it has been shaved off during microtomy. On the remaining bridges the stem is located in a region of the reconstruction (the ladder rung) that has particularly low resolution.

In addition to the sigmoid shape, the lead bridges have the following features in common. (*a*) At the contour cutoff chosen for display, they are ~13.5 nm in axial extent, a dimension large enough to contain two myosin heads. (*b*) They are dense features indicating a high degree of regularity due to positional order as well as high head occupancy within the cross-bridge lattice. (*c*) Lead bridges have a distinctly triangular shape, again suggesting a composite of two myosin heads.

The triangular shape is the most pronounced feature of the lead bridge. In simplest terms, it can be described as having one vertex at the cross-bridge origin on the thick filament and the opposite edge in contact with the thin filament. The forward edge of the triangle lies closest to the M line and is angled at ~45° to the filament axis, while the trailing edge lies closest to the Z line and is angled nearly perpendicular to the filament axis. The sectioning process affects the triangular shape of the lead bridge on Z by shaving away the stem portion of the neck-stem. Despite this, its triangular shape remains well-defined by the remaining portions of the forward and trailing edges which can be extrapolated to the missing vertex.

In some views (see Fig. 11 *a*) the angled forward edge shows an inflection toward perpendicular where it nears the thin filament. The fact that a similar inflection was seen in the myac layer lead bridge strengthens the possibility that it correlates with the short region of the myosin heads seen extending at nearly 90° from the filament axis in higher resolution views provided by acto-S1 3-D reconstructions (Vibert and Craig, 1982; Toyoshima and Wakabayashi, 1985; Milligan and Flicker, 1987; see also Fig. 5 in Amos, 1985).

Each lead bridge triangle is composed of two smaller components: its neck-stem and its portion of the midsegment. The triangular aspect of the midsegment is particularly easy to visualize in the surface images of the Z filament at 0° and −40° (Fig. 6, *a* and *c*). The triangular neck-stem can be seen best on the N filament at 0° and +42° tilt orientations (Fig. 6, *b* and *c*). Note that in the surface view corresponding to a −40° tilt, the plane of the neck-stem triangle appears rotated 20° relative to the filament axis. This rotation places the trailing edge closer to the thick filament surface than the leading edge just as noted in myac layers (Taylor et al., 1989).

The triangular shape of both midsegment and neck-stem is expressed in contoured sections calculated normal to the filament axis as changes in the sigmoid profile of the lead bridge in successive sections (Fig. 7). The sigmoid is most pronounced in the portion closest to the Z line. Profiles of both neck-stem and midsegment become shorter as these sections sample regions progressively closer to the M line. Towards the M line side of the bridge, the neck-stem profile disappears, leaving only the oval-shaped mass of the midsegment. In the interdoublet gap the unbridged thin filament has a circular profile. It is important to note that the midsegment shows little if any rotation through the 12–13-nm axial extent of the bridge (Fig. 7).

The rear bridges have the following features in common. (*a*) They are about half the axial length of lead bridges and have a simpler shape. This suggests that on average they contain one myosin head. (*b*) Their density is lower than that of the lead bridges and varies much more between the three axial levels within the 116-nm period. At two levels, the rear bridge density is reasonably high, while at the third, the rear bridge density is low (Fig. 8). The low and variable density of the rear bridges indicates less regularity in the location of the rear bridges and/or decreased occupancy of available sites for rear bridges. (*c*) Rear bridges are less tilted than lead bridges.

Evaluation of rear bridge tilt is more complicated for actin layers than for myac layers because some portions of rear bridges, i.e., on N filaments, are not included in the section. The rear bridges on N are oriented approximately normal to the section plane. As a result a portion of their neck-stem has been removed during microtomy so that bridge tilt would have to be measured from an incomplete length of cross-bridge. On the Z filament, rear bridges are fully presented in actin layers and can be used to estimate bridge tilt. In surface view (Fig. 6 *a*), rear bridges on the Z filament appear to extend from the ladder rung to the thin filament with little tilt.

Lead and rear bridges are separated with a gap of variable size (the interdoublet gap). These variations in intradoublet gap are best visualized on the N filament where rear bridges extend out of the plane of the section and can be viewed free of the ladder rung (Fig. 6). In one case (at level 3 on N) the intradoublet gap is clearly resolved while at the two adjacent levels, rear bridges merge smoothly with lead bridges leaving virtually no gap.

The presence of the intradoublet gap indicates that often, lead and rear bridges are separated by an unoccupied actin monomer. The presence of this unoccupied actin monomer in a region where two myosin heads are presumably avail-

Figure 6. Stereo surface views at different tilt angles of the actin layer reconstruction done in the two-sided plane group p1. The contour cutoff here is the same as that of Fig. 5. These three views cover the range of tilts illustrated in Fig. 9 here and also in Reedy and Reedy (1985, their Fig. 9 *b*). (*a*) View oriented at an axial tilt of −40°. In this orientation, the midsegment of the lead bridges and the neck-stem of the lead bridge on the Z filament are nearly parallel to the direction of view. (*b*) Untilted orientation. (*c*) +42°. This view is nearly parallel to the midsegment of lead bridges on Z filaments (located at level 2). Two equatorial repeats are shown, one of which has lead and rear bridges labeled for identification purposes. There are three axial levels at which cross-bridges form. Level 1 occurs on the "ladder rung", levels 2 and 3 are spaced approximately 12.9 nm apart between successive ladder rungs. Note diagonal rows (/) of cross-bridge features (labeled *R-L-R-L*) crossing the near surface from N to Z. These mark the actin targets that form a left-handed helix around excluded thick filaments on the near side of each N–Z pair in the actin layer. Ladder rungs form a blunted "V", which in freeze-fractured actin layers (Heuser, 1987, his Fig. 9 *a*) often shows an unpredicted elongation of the right limb. In contrast, our reconstruction shows ladder rungs symmetrical in length, consistent with all other 3-D information about these structures. We concur with Heuser's explanation that the elongation must be a metal-shadowing artifact which "extends" the right arm of the "V" to merge it with the prominent anterior protrusion of L bridge on Z (at level 2).

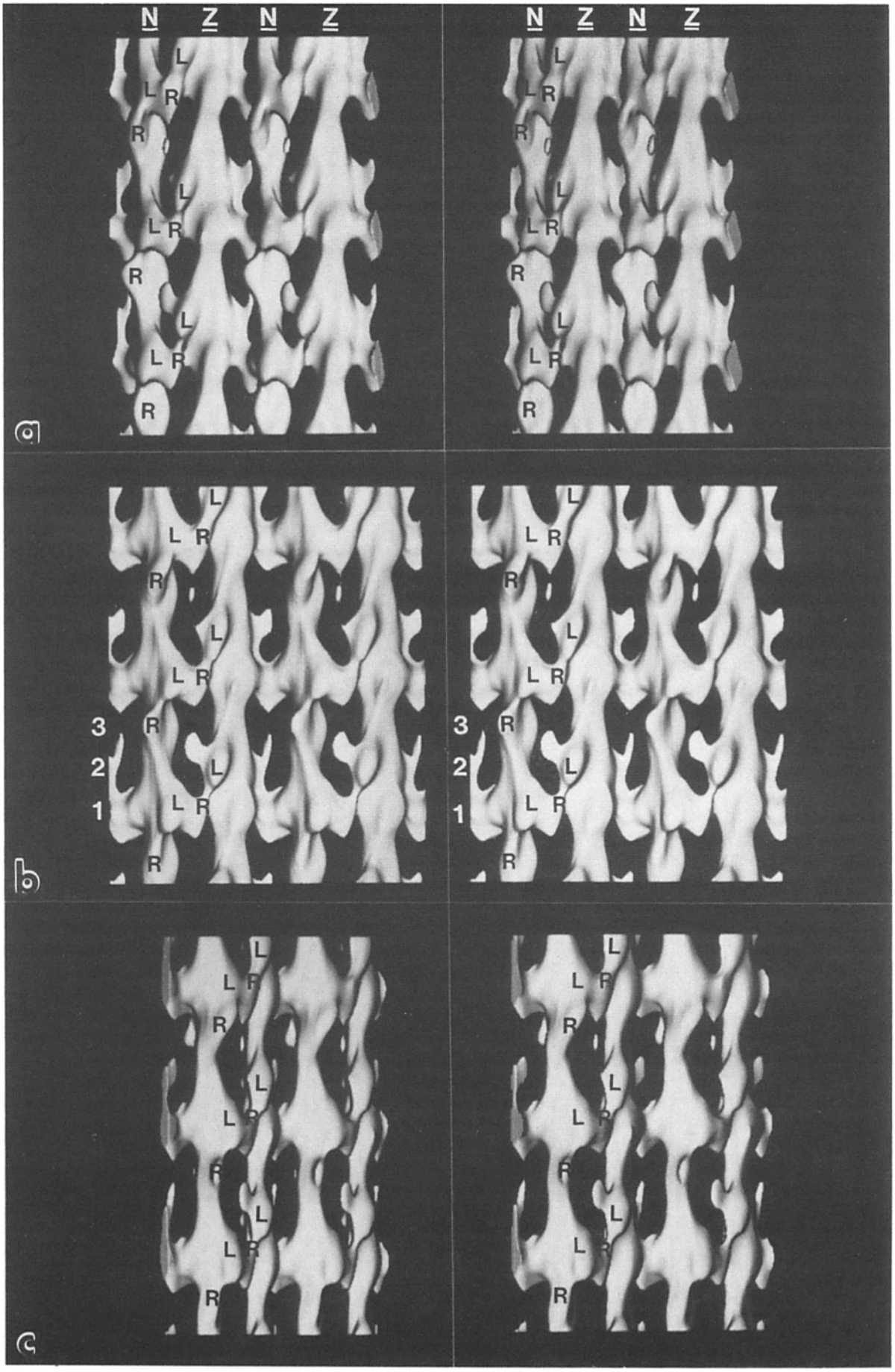
N Z N Z
N Z N Z
a
b
c
3
2
1

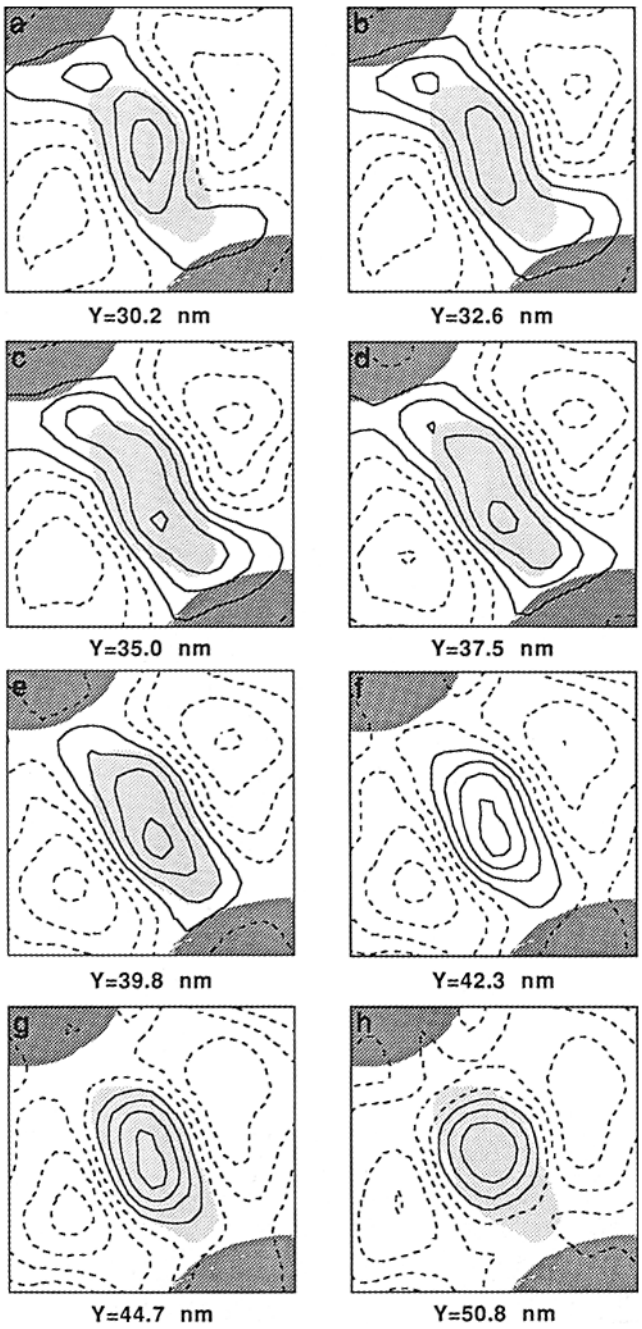

Figure 7. Contoured sections through the lead chevron of the thin filament reconstructed by averaging together N and Z. *a–g* cover a distance of 14.5 nm. Frame size is 30 × 30 nm. The outermost solid oval outline from *f*, representing the minimal dimension of the midsegment of the chevron, has been overlaid on the outer sections (pale grey stippled area) to illustrate the relationship of the neck-stem with the midsegment. Positions of thick filaments are indicated by dark grey stippling at upper left and lower right. *h* is a section through the interdoublet gap, a region devoid of cross-bridges.

able, yet only one binds, is an expression of the interplay of lattice effects and actin azimuth that ultimately determine where the myosin heads will bind. However, the variable size of the intradoublet gap indicates that some fraction of rear bridges are not separated from lead bridges by an unlabeled actin. These variations in intradoublet gap are compatible with the size of the target zone on each thin filament long pitch helix, originally proposed to be three to four actins in length (Reedy, 1968). The simplest interpretation that encompasses variations in both intradoublet gap and rear bridge density is that rear bridges contain only a single myosin head distributed in the filament lattice over two actin monomers and that rear bridges do not occur at every rear bridge level. How is the 116-nm period expressed, since there is no clear feature repeating at 14.5 nm? This reconstruction suggests that the variable density of rear bridges and the variable width of the intradoublet gap constitute the major manifestations of the 116-nm repeat close to actin.

In the ladder rung, origins of lead and rear bridges merge near their contacts with the excluded thick filament. The ladder rung itself becomes broader with increasing distance from the central plane of the reconstruction. Other effects could also contribute to this broadening. It may represent mass from the thick filament surface included in the actin layer section, or, it may be a manifestation of the low resolution normally expected at the surface of the reconstruction.

Comparison with Projections of Tilted Actin Layers

The cross-bridge arrangement in the actin layer was deduced by Reedy and Reedy (1985) from tilted sections. To facilitate comparison, we have calculated projection maps and matched surface views of the reconstruction at the same orientation as original and optically filtered images reported in the earlier work. The images produced, however, differ from those in Reedy and Reedy in that unsampled layer lines at 5.9 and 5.1 nm are not included.

Axial tilts produce characteristic alterations in the appearance of thin filaments and cross-bridges. The projected density of the cross-bridges changes in a tilt series from a single dense bead over actin, referred to as center beading, to a pair of dense beads flanking actin and separated by up to 8.5 nm, referred to as straddle beading. Center beading and straddle beading are expressions of the shape of the cross-bridge–actin rigor complex. Center beading developes in axial tilts when the projection direction is aligned with the long axis of the midsegment. Straddle beading occurs when the projection direction is down the long axis of the neck-stem domains. Center and straddle beading are important properties of projected images of paired cross-bridges in longitudinal sections. The relative prominence of center or straddle beading in the separate micrographs affect the resultant shape of the cross-bridges in the 3-D reconstruction, because tilt restrictions may exclude or limit the contribution of one or the other projections to the collected data.

The origin of center and straddle beading can best be seen for the lead bridge on Z (level 2) by comparison of matched surface displays (Fig. 6) and projections (Fig. 9). In the untilted actin layer the projection image of this lead bridge appears as a pair of closely spaced, extremely dense beads that are elongated and slanted. The corresponding surface view (Fig. 6 *b*) shows the lead bridge necks extending out from the plane of the section roughly parallel with the direction of view. These straddle beads become sharply defined at −18° (Fig. 9 *b*) but decrease in density at −40° as the bridge necks rotate across the field of view. At positive tilt angles, straddle beading converts to center beading (Fig. 9, *d* and *e*). The corresponding 3-D image illustrates the alignment of the midsegment axis with the projection direction (Fig. 6 *c*).

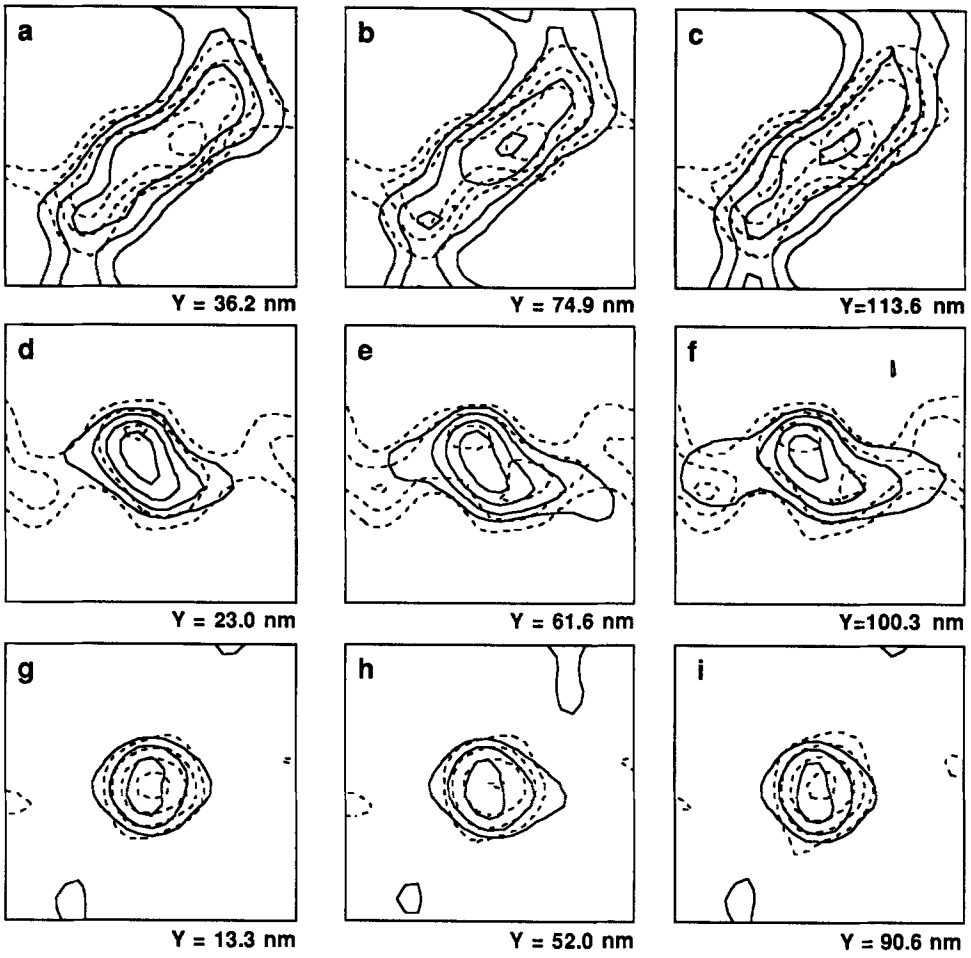

Figure 8. Contoured sections perpendicular to the filament axis comparing Z and N filaments. Solid lines are contours through the N filament and dashed lines are contours through the Z filament. Sections are displayed after reorienting Z for optimum rotational and translational alignment with respect to N. Both thin filaments have been stretched normal to the section plane to compensate for section thinning. Frame size is 30 × 30 nm. *a–c*, sections through the lead bridge; *d–f*, sections through the rear bridge; *g–i*, sections through the interdoublet gap.

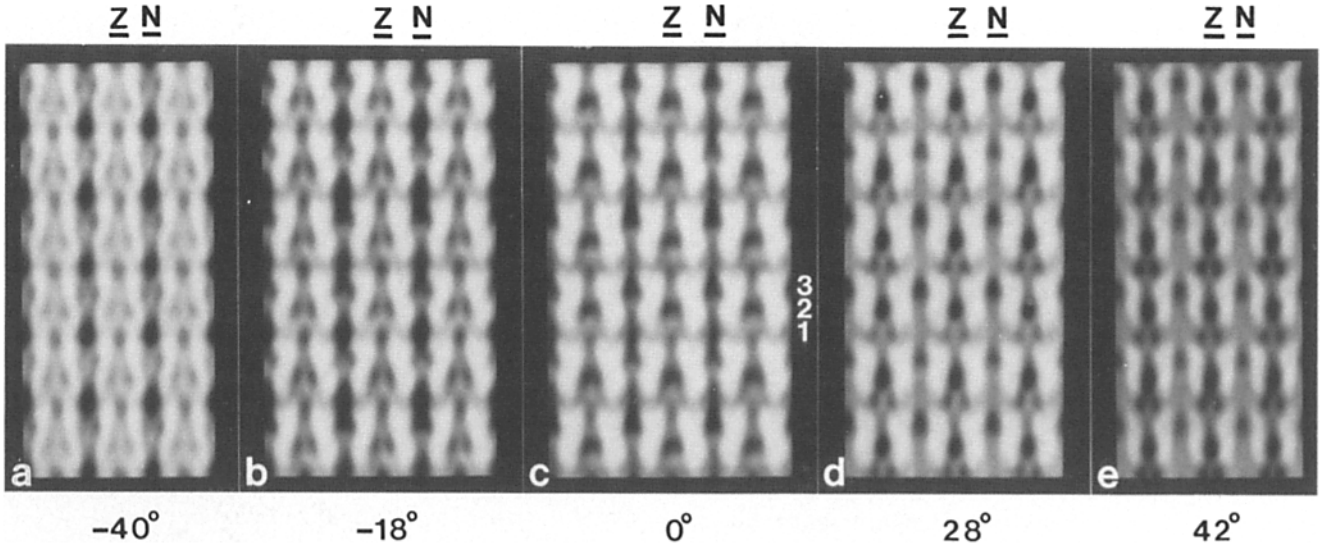

Figure 9. Selected projections of the actin layer 3-D reconstruction. These five projections are identical in orientation to the optically filtered images shown in Fig. 9 *b* of Reedy and Reedy (1985). They illustrate the development of center beading and straddle beading in axial tilts of actin layers. (*a*) View oriented at an axial tilt of −40°. Center beading is particularly pronounced at level 1 in this panel. (*b*) −18°. Straddle beading at the lead bridge is clearly illustrated at level 2. (*c*) Untilted orientation. Neither center beading nor straddle beading are well-developed in this orientation. (*d*) +28°. Straddle beading on Z is clear at the rear bridges on level 1. (*e*) +42°. The lead bridge on N at level 1 is of low density while center beading on Z at level 2 is well developed, and is fading on N at level 3. Three equatorial and two axial repeats are shown.

Two features of the 3-D reconstruction are notably affected by the prominence of center and straddle beading in projection images of tilted sections and by the angle limitations of the tilt series data. Lead bridges on Z appear more sigmoidal than those on N (Fig. 8) because straddle beading plays a larger part in their tilt series views. Within a tilt angle range of −40° to +42° both center and straddle bead images are readily obtained for this bridge (Fig. 9). At the lead bridge on N, straddle beading never fully develops even within the 60° tilt limit. Its less prominent sigmoid shape can thus be explained by the dominance of center over straddle beading in the tilt series image data of that cross-bridge.

The density across the filament axis is also partly dependent on center and straddle beading. In the 3-D reconstruction obtained from tilt series data alone (not shown) lead bridges on Z, which displays both center and straddle beading in their tilt series images, have lower density across the thin filament axis than those on N, where the density stays relatively constant. Lead bridges on N display only center beading in their tilt series images. The thick section data contributes to alleviating the differences at the lead bridge between N and Z by providing data within the missing cone. By far the dominant contribution of the thick section data comes from the actin rows which complete the equatorial plane of the actin layer transform. Even with the actin row data, some density differences across the thin filament persist. The actin columns should contain a straddle bead view of the lead bridge on N, albeit superimposed on the center bead of the rear bridge on Z, but apparently the contrast or resolution of this view in the actin columns is insufficient to greatly affect the reconstruction. Related effects of both center and straddle beading and of thick section data can be seen in the myac layer reconstruction, whose projections are dominated by straddle beads at the lead bridges, and which in the absence of thick section data had very low density on the thin filament axis (Taylor et al., 1984*b*).

The projected images of both rear bridges (level 3 on N and level 1 on Z) are converted from center beading to straddle beading within the available tilt range (Fig. 9) allowing full expression of the sigmoid shape in the 3-D reconstruction (Fig. 8). Both the center and straddle beads at the rear bridges are much less elongated axially than those of the lead bridges.

The conversion of straddle beading to center beading at the rear bridges is accompanied by a small shift (~1 nm) of the peak of the projected density towards the Z line. This feature has now been recognized in tilt series views of numerous actin layers (e.g., Fig. 18 in Reedy and Reedy, 1985). This Z-ward shift of the center bead density is opposite to the M-ward shift expected if the neck-stem domains were tilted at the 45° rigor angle and is unexpected even for the relatively untilted rear bridges observed. This shift suggests that an additional element is present in this part of the structure. Possibly troponin is responsible for this phenomenon. Although there is no clearly resolved feature which can be identified with the density shift, a shoulder is visible in the 3-D reconstruction at each rear bridge level appearing more pronounced on Z than on N (Fig. 6 *a*).

Averaged Thin Filament

Averaging N and Z filaments together should result in an image with a 40% noise reduction. The N and Z filaments are related through the space group symmetry of the hexagonal lattice of rigor insect flight muscle which is either $P6_5$ (Wray et al., 1978) or $P6_4$ (Holmes et al., 1980). In either space group, adjacent thin filaments such as Z and N in actin layers can be aligned by rotating Z 60° counterclockwise about the filament axis and translating it axially by −12.9 nm. We tested this symmetry relationship and found that it is preserved overall in this reconstruction.

To test the relationship between the thin filaments in the reconstruction, we calculated correlation coefficients for the two filaments at different relative rotations and axial translations. For these results to be meaningful, some correction must be made for mass loss and the resultant section thinning. Compensating for section thinning by stretching the reconstruction in the Z direction resulted in better correlation coefficients between the two filaments. For the uncorrected reconstruction, the maximum correlation coefficient was 71%. The best coefficients were obtained from maps stretched by factors of 1.5 to 1.7 which gave coefficients of 85%. Some correspondence is expected between the best correction factor found from the filament correlation and the factors of 1.7–1.8 used in aligning and merging the actin column and actin row data with the tilt series data. The difference between these values is probably due to section compression, which was not corrected for, and which reduces the interfilament spacing by 11% from the 52-nm present in the fixed and embedded tissue block.

The rotational correlation analysis showed that the transformation which best aligned the Z filament with the N filament was obtained for a counterclockwise rotation of 67° and an axial translation of −13.3 nm. This transformation does not differ significantly from the predicted values. The rotation angle in this transformation bears an unfortunate numerical similarity to the completely unrelated issue of the number of flared-X levels in the 116-nm axial repeat; eight successive flared-X levels separated by 14.5 nm would have a rotation of 67° while nine successive levels would have a rotation of 60°.

Using the transformation obtained by the correlation analysis, we have reinterpolated the reconstruction to produce an image of Z aligned with N for comparison (Fig. 8) and for averaging (Figs. 7 and 10). This averaging of N and Z thin filaments accentuates several features of the reconstruction. The triangular shape of the lead cross-bridge is more pronounced in the averaged thin filament image. The rear bridges are (*a*) oriented more perpendicular to the filament axis, (*b*) vary more in density along the 116-nm repeat than in either of the individual filaments, and (*c*) are better resolved from lead bridges. Coincident with the better resolution of the rear bridges is better definition of the intradoublet gaps. The sigmoid shape of the averaged lead bridge is naturally intermediate between that seen individually on N or Z.

The Question of Thin Filament Twist

In the actin layer reconstruction the thin filament is not resolved from the cross-bridges. However, the bridging density should reflect the underlying helical structure of the thin filament as long as the spatial relationship between the myosin head and its actin monomer is identical for all cross-bridges. Based on this assumption, there appears to be a tendency for density near the thin filament to show different

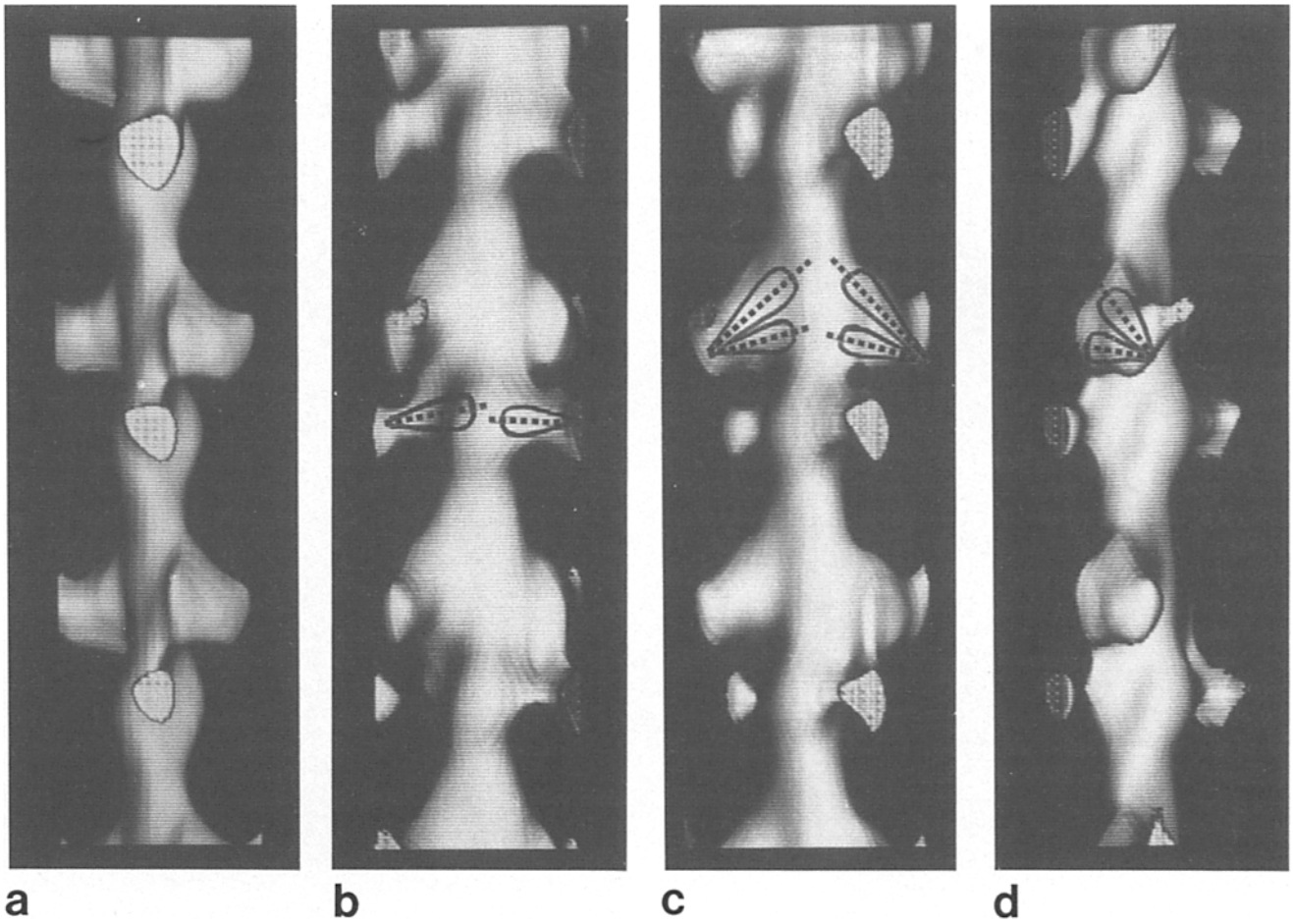

Figure 10. Surface display of the thin filament reconstruction produced by averaging optimally aligned Z and N structures. (*a*) Viewed from the orientation of N filament in untilted actin layer. (*b*) Orientation of untilted myac layer. (*c*) View rotated to present flat view of the triangular lead bridge neck-stem. (*d*) Orientation of the Z filament in untilted actin layer. Sketched onto the last three sections are the inferred orientations of the heads in the cross-bridges. The dashed line is the centerline of the head.

degrees of twist at the different bridging levels. This was pointed out earlier in connection with the contoured map sections through the lead bridges (Fig. 7). In a thin filament uniformly twisted we would expect a rotation of 26° per actin monomer, which is equivalent to an axial translation of 5.5 nm. The lead bridges extend axially through 12–13 nm of the map and by virtue of their size should encompass about two actin monomers each. Yet through this 12–13-nm distance the contoured sections through the lead bridges show little if any rotation of the midsegment of the bridge, i.e., the portion containing the thin filament and actin binding domains of the myosin head.

A quantitative and objective measure of variations in thin filament twist of rigor actin layers was obtained by rotational correlation with S1-decorated actin, a structure which exhibits smooth and uniform twist. A helical projection from an acto-S1 helical reconstruction (Taylor and Amos, 1981) was used to represent the density distribution in the bridging regions of the reconstruction. This motif was cross-correlated at different rotations with map sections through N and Z thin filaments to generate plots of rotation angle for best alignment. There are two limitations to this analysis. First, no single motif can represent both lead and rear bridges, which differ from each other in both tilt and slew (Taylor et al., 1984*b*, 1989). Second, the acto-S1 reconstruction was obtained from muscle thin filaments decorated with chymotryptic S1 and thereby lacks LC2 which is present in *Lethocerus* myosin (Bullard et al., 1973; Lehman et al., 1974). The acto-S1 helical projection nevertheless has the sigmoid shape which is the most pronounced feature of the cross-bridges at low resolution.

The quantity measured was the rotation angle at which the helical projection best matched the thin filament density, tested at successive axial positions separated by 1.21 nm. For a uniformly twisted helix, the expectation is that the plot of rotation angle versus axial position would be linear, at least within the bridging region, and have a slope of 4.7°/nm. The curves obtained generally show three regions of differing twist (Fig. 11): (*a*) one region, encompassing the rear bridge, appears with a slope very nearly equal the expected value, (*b*) at the lead bridge the slope decreases markedly indicating a region of effectively no twist, and (*c*) at the forward edge of the lead bridge and continuing into the interdoublet gap apparently conflicting results were obtained for the two filaments. By implication this third region should have higher than average twist to compensate for what appears to be un-

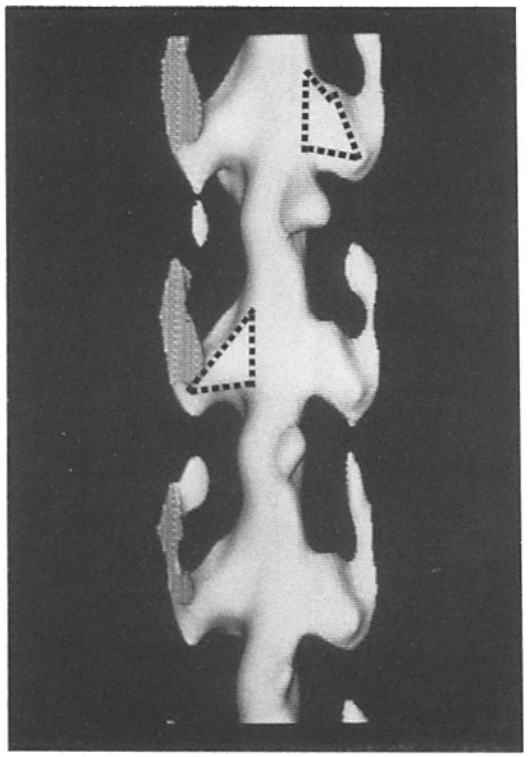

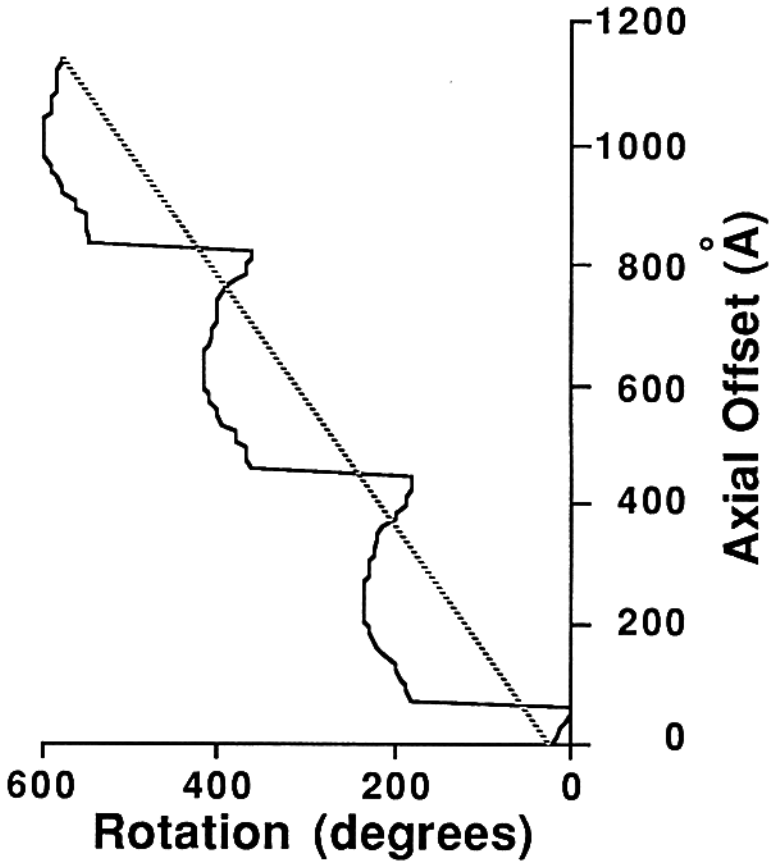
1200
1000
800
600
400
200
0
Axial Offset (Å)
600
400
200
0
Rotation (degrees)

a

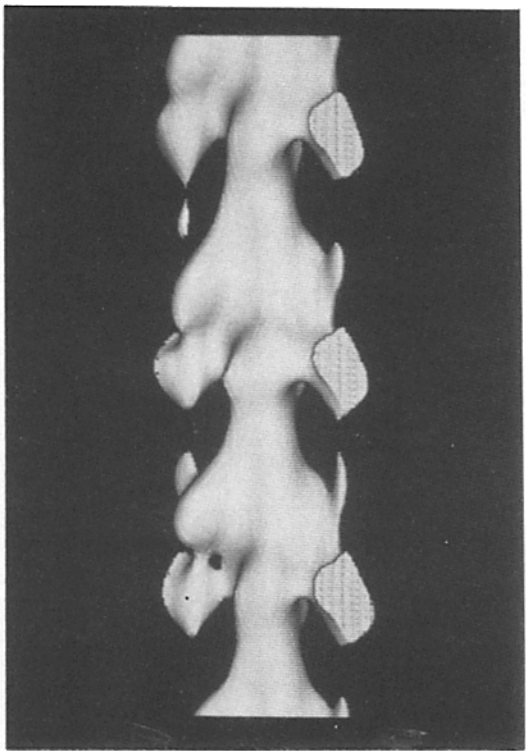

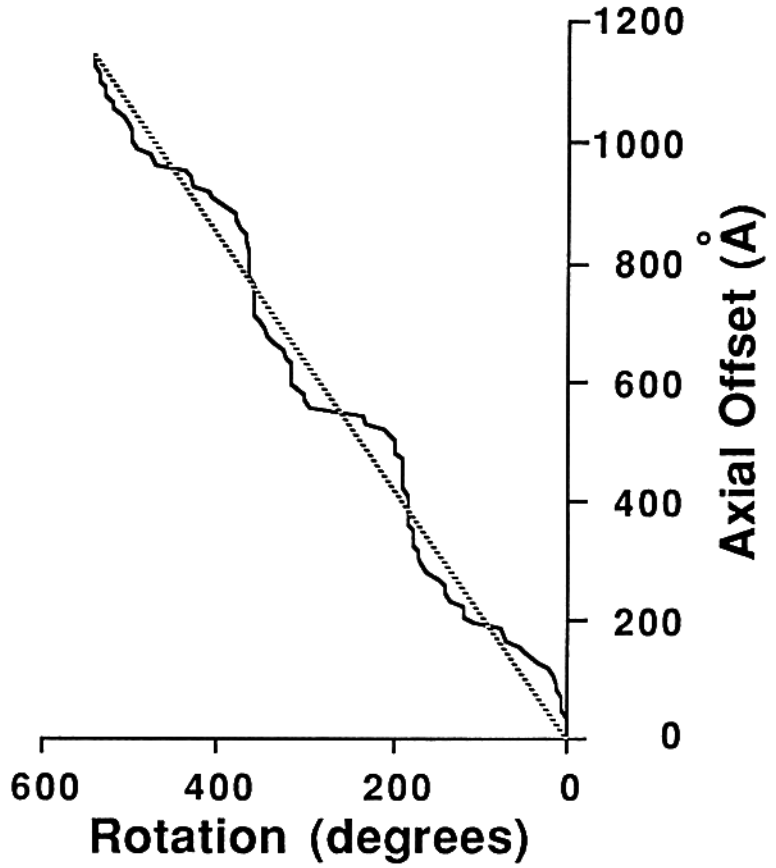
1200
1000
800
600
400
200
0
Axial Offset (Å)
600
400
200
0
Rotation (degrees)

b

dertwisting at the lead bridge and yet maintain the 38.7-nm actin repeat. In fact, in this region on the Z filament the slope increased markedly indicating greater than average twist, but for the N filament the slope decreased still further suggesting that the twist had reversed hand (left handed). This is a particularly clear instance of the effect already discussed where, in the absence of cross-bridge density, non-cross-bridge features lead the rotational alignment to jump from one long pitch strand to the opposite strand (Taylor et al., 1989).

The twist variations in the thin filament can also be illustrated using contour plots of cylindrical sections (Fig. 12). These show one region with normal twist for a 28/13 helix, identifiable with the rear bridge, and another region that appears undertwisted, identifiable with the lead bridge. By implication, a third region should be hypertwisted. The implied hypertwist region appears only at the Z filament at 7.0 nm radius just Z-ward of the plotted position of the rear bridge. Undertwisting appears more pronounced at the N filament. It is worth noting here that both the cross-correlation analysis and the cylindrical section plots suggest that cross-bridge density through the rear bridge and into the trailing portion of the lead bridge follow the predicted actin helix reasonably well while it is the forward head of the lead bridge that appears to be out of step with the actin helix.

The apparent hypertwisting observed at the Z filament in these cylindrical sections is associated with a rather pronounced density peak at 7.0 nm radius just Z-ward of the rear bridge (Fig. 12 *a*). At 7.0-nm radius, this peak cannot be due to actin or tropomyosin which should be contained within a cylinder of radius 5.0 nm, and it is not a cross-bridge. It possibly represents troponin. This feature can be identified as the pronounced shoulder seen in the surface views at the rear bridge especially on the Z filament (Fig. 6, *a* and *b*). It also correlates well with the Z-ward shift of the rear bridge center beads in the projection images (Fig. 9).

Discussion

Two Classes of Rigor Cross-Bridge

The significance of the actin layer reconstruction is that it confirms and extends the observations on rigor cross-bridge structure made from the myac layer, and does so in an independent and objective fashion, because the actin layer reconstruction represents data from a totally different image context and shows cross-bridges from two complementary viewing directions, both different from the single view available in myac layer sections. The most striking common theme of these reconstructions is the demonstration of two forms of rigor cross-bridges. These forms differ in tilt, size, density, and shape. Each form is associated with a region of apparently different thin filament twist.

One cross-bridge class, the rear bridge, is small and is oriented nearly perpendicular to the filament axis. The size and shape of the rear bridges suggest that each consists of a single myosin head. Rear bridges have lower density that lead bridges. This reflects the fact that there are insufficient myosin molecules to occupy each rear bridge subtarget. Rear bridges display noticeable variability in both density and separation from lead bridges at the three chevron levels within the unit cell. These variations in average density arise from two causes. (*a*) They may reflect different frequencies of rear bridge formation and hence different average mass at each rear bridge level. (*b*) Density variations may also arise because the single myosin head binds to only one of the two actin monomers within each rear bridge subtarget. This delocalizes the contribution of the single head in the 3-D image and gives rear bridges a low average density. In addition, this delocalization leads to variability in size of intradoublet gap if these two actin monomers in the subtarget are occupied at different relative frequencies within each of the three axial double chevron groupings. This variability in both density and separation from lead bridges is the most visible manifestation of the 116-nm axial period. In addition, rear bridges occur in regions of the thin filament having apparently normal twist.

The other cross-bridge class, the lead bridge, is a large dense structure with an axial extent of ~13 nm and an overall triangular shape. This shape encompasses both a triangular neck-stem and a triangular portion of the midsegment. The neck-stem triangle consists of a forward edge (closest to the M line) oriented at about a 45° angle relative to the filament axis, and a trailing edge (closest to the Z line) oriented perpendicular to the filament axis. The plane of the neck–stem triangle is rotated ~20° relative to the filament axis in such a way that its trailing edge lies closer to the thick filament surface than the forward edge. The triangular shape of the rigor lead bridge is also observed in (*a*) the 3-D reconstruction of the rigor myac layer (Taylor et al., 1989), (*b*) oblique section reconstructions of 15-nm cross sections (Taylor, K. A., M. C. Reedy, M. K. Reedy, and R. A. Crowther, unpublished observations), (*c*) numerous cross-bridge structures observed in swollen rigor IFM fibers (Reedy et al., 1988*a*).

The triangular lead bridge shape can most easily be interpreted as resulting from two heads of one myosin molecule bound to successive actin monomers on one thin filament. The forward edge of this cross-bridge has the 45° slope long identified with angled rigor heads, but the 90° slope of the trailing edge indicates less tilt for the second head. The triangular shape need not require that the two myosin heads have exactly the same measured tilt as their associated edges, because the club shape of the myosin heads themselves could exaggerate a lesser mean tilt for the forward head and a greater mean tilt for the trailing head. The shape of the lead bridge can be approximated with a pair of club shaped motifs

Figure 11. Plots of the rotational alignment of the acto-S1 helical projection with the two thin filaments of the actin layer reconstruction. To the left of the plots are displayed surface views of the two thin filaments shown in approximately the myac layer orientation. Both the graphs and the surface views are vertically aligned for ease of comparison. These plots are typical and represent a cross-correlation between actin layer maps stretched to correct for section thinning by a factor of 1.8 and a helical projection calculated with full weight equator and layer lines 2,4 and 6 of the acto-S1 transform. The dashed line represents the path of the long-pitch helices for an ideal 28/13 helix. (*a*) N filament; (*b*) Z filament.

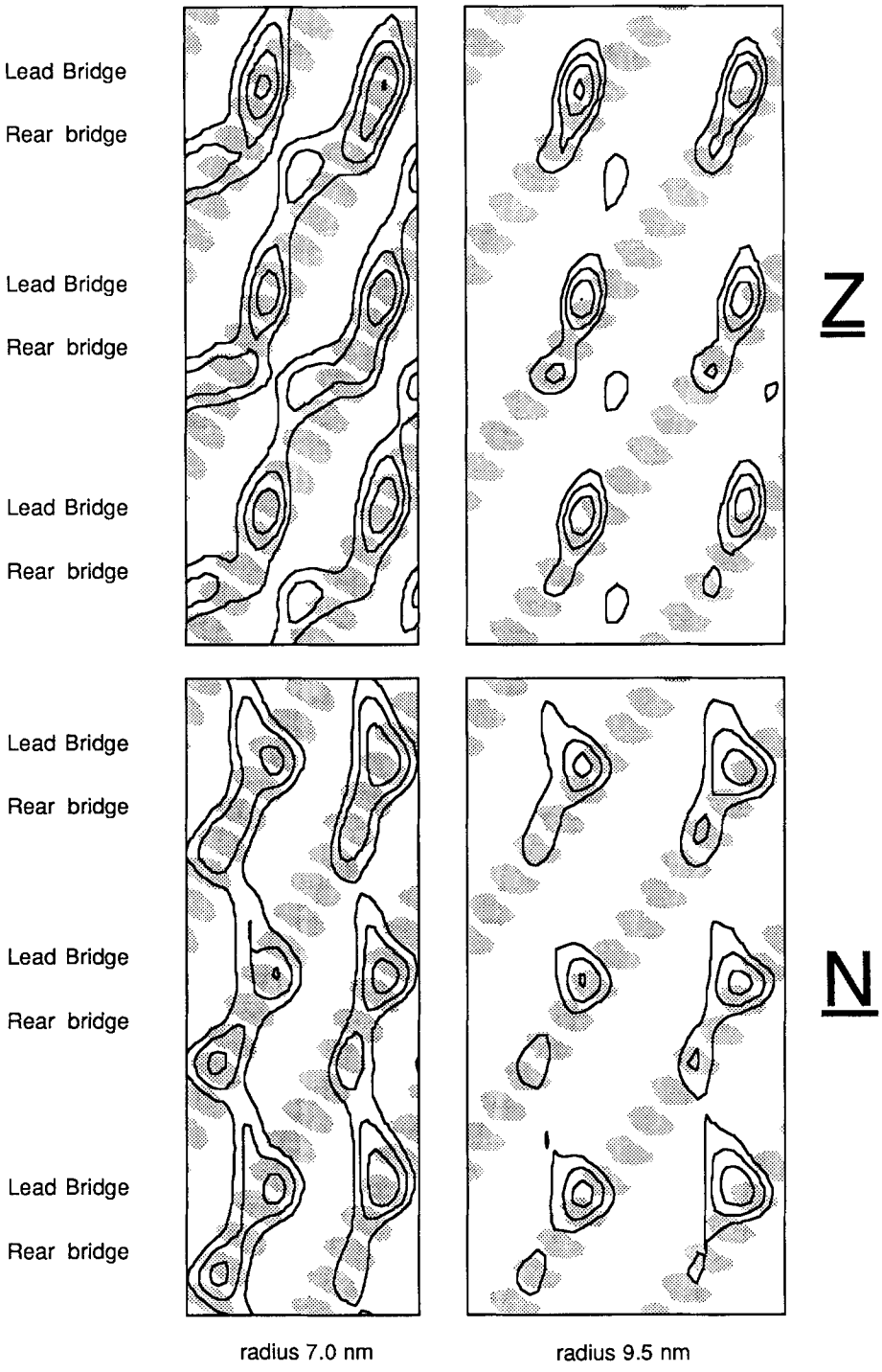

Figure 12. Plots of cylindrical sections at 7.0 and 9.5 nm radii about the actin layer thin filaments. Solid lines are the actin layer contours starting with the same cutoff used for the surface images of Fig. 6. For the cylindrical section calculation, the actin layer reconstruction was stretched by a factor of 1.8 normal to the section plane to compensate for section thinning. Shaded areas are cylindrical sections calculated through an acto-S1 reconstruction (Amos, 1985) which illustrate both the relative sizes of S1 with respect to lead and rear bridges and the behavior of a regular 28/13 helix. The maps show a full 116-nm axial period and have been scaled in the horizontal direction to give the true circumference. The top two sections are through the Z filament, the bottom two sections are through the N filament.

in which the forward head has an angle of 48° while the trailing head has an angle of 77° (Fig. 10).

The triangular shape of the lead bridge has several implications for myosin head conformation in two headed cross-bridges. First, to account for this triangular shape the neck domains of the two heads must be relatively rigid and inelastic thereby preventing the two heads from reaching similar tilted configurations. If the two heads within the lead bridge had similar tilt angles, we would expect a shape more rectangular than triangular. Second, the lack of twist at the midsegment of the lead bridge, as well as the shape and rotation of the neck–stem triangle suggests that the two heads differ not only in tilt angle, but also in the way they are bent azimuthally within the complex. Based upon the interpretation that the lead bridge consists of two heads of one myosin, its shape could be due to the divergence of the two heads from a common vertex and their termination at different axial positions on the thin filament. The two termini differ in axial coordinate by 5.5 nm. However, their azimuthal coordinates appear the same, rather than differing by 26° as would be expected if the thin filament displayed conventional twist. The two heads are also bent differently under these structural

constraints. If equivalent contour length is to be preserved in both heads, the trailing head must bend at a point further from the thin filament than the forward head. This means that it contributes a greater portion of its length to the midsegment and a smaller portion of its length to the neck–stem triangle than the forward head.

That rigor has only a single, uniform cross-bridge angle is consistent with the narrowly defined range of probe angles observed in electron paramagnetic resonance experiments (Barnett and Thomas, 1984; Thomas and Cooke, 1980; Thomas et al., 1983). This same narrow range is also observed for attached myosin heads in contracting muscle (Cooke et al., 1982). These observations have led to the conclusion that at least part of the myosin head attaches to actin at the same uniform angle in rigor and in contracting muscle (Thomas, 1987). A uniform angle for the actin binding domain of myosin can be reconciled with the differing bridge angles observed here by a point of flexion at the junction between neck and actin binding domain. However, to account for the differing lengths of midsegment and neck domains at the forward and trailing edges of the lead chevron, an additional point of flexion seems necessary somewhat closer to the vertex of the two heads. If there are two different points of flexion in each myosin head, this implies an additional interjoint domain in the region of the head–neck junction. This interjoint domain may correspond to the middle domain observed in electron micrographs of myosin molecules (Walker and Trinick, 1988).

Model calculations of x-ray diffraction patterns from IFM have been used to infer the cross-bridge tilt angle in rigor (Miller and Tregear, 1972; Rodger and Tregear, 1974; Holmes et al., 1980). To a first approximation x-ray diagrams can be modeled by rod or club shaped myosin heads of uniform size and angle. The fact that reasonable agreement can be obtained under this set of assumptions does not necessarily conflict with our conclusion of differing head conformations. The uniform tilt angle found optimum in these model calculations is intermediate between 45° and 90° which suggests to us that it could well be an average of the different head angles observed here. Studies are in progress to model the x-ray data using two cross-bridge forms.

The demonstration of two rigor tilt angles complicates the assignment of a single tilt angle to the rigor state. Initially, Reedy et al. (1965) described rigor cross-bridges angled at 45°. Since that time, 45° angled heads have served as a model for the end of the power stroke (Huxley, 1969). However, improved fixation (Reedy and Reedy, 1985) and 3-D reconstruction (Taylor et al., 1984*b*) revealed differences in tilt angle distinguishing two classes of in situ cross-bridges. Helical reconstructions of acto-S1 have also served as models for the tilt angle of rigor cross-bridges and until recently appeared to suggest tilt angles of 40–55° (Moore et al., 1970; Vibert and Craig, 1982; Taylor and Amos, 1981). More recently, Toyoshima and Wakabayashi (1985) have argued that S1 consists of two segments. One of these contains the actin binding region of the S1 and is tilted at ~65°. We would identify this with a portion of the midsegment of the cross-bridge. The other, which we would identify with the bridge neck, is tilted at ~18°. The most recent reconstruction (Milligan and Flicker, 1987) suggests an overall tilt angle through the longest chord of 42° but also reveals (by our interpretation) a head with two segments at different angles.

The differing angles of lead and rear bridges that we observe are most likely enforced by lattice constraints on cross-bridge conformation in situ. One of these arises from the alignment of surface lattices between cross-bridge origins on the thick filament and the actin target lattice. A second constraint would arise if there is a temporal sequence in cross-bridge formation during rigor induction as previously suggested (Taylor et al., 1984*b*). This temporal sequence is envisioned to account for the sorting of cross-bridge forms into two classes and need not imply that all cross-bridges of these two types form synchronously, but rather implies that asynchrony is not totally random. Under any model of asynchronous cross-bridge formation, one would expect restrictions on filament sliding to result from earlier attached cross-bridges that form permanent rigor bonds. For example, if rear bridges as a group form later in rigor induction, they may be prevented from tilting to 45° because of the resistance to filament sliding resulting from earlier attached lead bridges.

Rigor cross-bridges once formed are resistant to distortion by stretch when examined by x-ray diffraction (Haselgrove, 1970; Naylor and Podolsky, 1981), paramagnetic resonance (Cooke, 1981), polarization fluorescence (Yanagida, 1984), and electron microscopy (Trombitas et al., 1988). If the cross-bridges were all single-headed it would seem intuitively possible that the tilt angle could be altered by stretch. We suggest that the apparent rigidity of rigor cross-bridges is conferred by two-headed cross-bridges. The triangular shape of these two-headed bridges lends the structure enhanced rigidity.

Changes in Thin Filament Twist

Twist alterations at the lead chevron midsegment are the most difficult aspect of the structure to interpret because the actin long pitch helical strands are not clearly resolved anywhere in these reconstructions. Just as S1 decoration amplifies the visibility of the F actin helical structure, we must rely here on the cross-bridges to reveal the helical structure of the underlying thin filament. The apparent twist variations can be summarized as a region displaying little or no twist at the lead bridge, a region of apparently normal twist at the rear bridge, and by inference, a region of compensatory overtwisting in the interdoublet gap that would be required to preserve the 38.7-nm axial period. Here we describe the twist variations as "apparent" because they could arise from effects other than nonuniform twist of the actin helix (Taylor et al., 1984*b*).

Several effects in the 3-D reconstruction process must be considered in evaluating these twist variations in the thin filament. Twist variation might be the result of the low axial resolution of the reconstruction which has the effect of smoothing the cross-bridge density axially. At this time we cannot exclude this possibility completely but it would seem unlikely. Smooth helical twist is actually the lowest resolution feature of the thin filament, since it can be defined by the 38.7-nm layer line alone. In fact, a fairly extensive part of the bridging region can be aligned along the predicted long pitch actin helix while only a relatively short region at the forward edge of the lead bridge deviates markedly from the predicted helical path. The twist variations might also arise in the reconstruction as a result of unmeasured transform

data within the missing cone. Although we obtain some of this data from the thick section images, there are regions, particularly the innermost parts of the 38.7-nm layer line, which are unobtainable. However, the missing cone should affect the myac and actin layer thin filaments differently because they each lie at different orientations relative to the section plane. Therefore, the fact that twist variations are consistently observed in each filament despite the presence of other structural differences between them argues against twist variations arising from the missing cone.

We interpret the lack of midsegment rotation in the lead chevron as an untwisting that reflects a mechanism for distributing strain in myosin brought on by two-headed binding to actin (Taylor et al., 1984*b*). F actin flexibility has been observed in several systems (Egelman et al., 1982, 1983; Stokes and DeRosier, 1987). The apparent alterations in actin filament twist suggested here appear as a localized untwisting of the thin filament because of the symmetrical distortion of the opposed cross-bridge pair. One might predict by extrapolation that saturation of actin with heavy meromyosin (HMM) should result in rather dramatic alterations in helical repeat. The fact that these helical changes are not observed (Huxley, 1963) could be due to unfavorable energetics but more likely is an expression of the highly localized nature of the distortion; it is restricted to the two actin monomers bound to the HMM. If this distortion were highly regular along the thin filament, saturation with HMM would at most give rise to density modulations with an 11-nm axial period without affecting the average pitch at all (Kajiyama, 1988). However, an 11-nm period might not be readily observed in acto-HMM because of the so called "parking problem" (Green and Eisenberg, 1980). This will result in long range disorder of the 11-nm period due to occasional single-headed binding of HMM or the presence of actin sites unoccupied by myosin heads.

The tethering of cross-bridges to the thick filament is the dominant constraint on in situ structure and affects both actin twist and myosin head conformation. It is also the factor that differentiates the in situ actomyosin structure from that in vitro. In both cases, the two heads are attached to a common vertex, but in vitro HMM has more freedom to achieve appropriate alignment with actin because it is not tethered to the thick filament. The departures from uniform S1 structure observed in situ such as the unusual bending of the trailing head and the associated twist variations in the actin filament, represent the optimal configuration for two headed binding under the particular lattice constraints operating in this muscle.

A scheme for distributing stress within the lead chevron suggests a mechanism for untwisting the thin filaments in situ. Under this scheme the common connection of two myosin heads enables the vertex to act as a fulcrum to distribute the stress among myosin heads and actin. Thus, the bending of the trailing head suggests a tendency to pull the vertex of the two myosin heads toward the thin filament. Such bending could apply a compressive force along the neck domain of the forward head. Because the forward head is tilted, this force would have two components. One component, in a plane perpendicular to the filament axis and tangential to the filament, would exert an untwisting torque on the thin filament. The other force component would be directed along the filament axis in the direction of sliding. The fact that lead bridges occur in opposed pairs in IFM insures that the torsional forces are applied symmetrically about the filament axis. The direction of the torsional force hypothesized here would account for the observation that the forward head of the lead bridge is out of alignment with the helical track defined by the trailing head and the rear bridge. In addition, under this scheme the actin binding domain of each myosin head would act as a lever to amplify the torsional force on the thin filament applied through the neck region of the myosin head.

An important question is whether the lack of midsegment rotation through the rigor lead bridge (the midsegment contains both actin and the actin binding domain of myosin) requires an alteration in the twist of the actin filament or may be explicable by some other native structural mechanism. Three possibilities suggest themselves. Troponin could contribute toward the apparent alterations in thin filament twist depending upon its shape and positioning relative to the cross-bridges. Troponin is so far not revealed conclusively in our 3-D reconstructions despite its large size (Bullard et al., 1988). Although not compelling, the evidence from these reconstructions tentatively places troponin nearest the rear bridge. Moreover, no alternative location is suggested by any other available data. If *Lethocerus* troponin resembles its vertebrate counterpart (Flicker et al., 1982) it could span the cross-bridge region. Much of its mass would then be spread out axially and would contribute little to any single feature of the reconstruction. However, a globular domain on troponin could produce a visible effect. Troponin mass centered at the rear bridge might explain why our earlier determination of helical variations (Taylor et al., 1984*b*) suggested greater than normal twist through the rear bridge region, whereas the current reconstructions suggest normal twist. The earlier conclusion was based on the rotations of centers of mass of features that we interpreted as actin long pitch strands. It is now clear that the position of these centers of mass can be affected by cross-bridges and possibly even troponin. However, the current assessment of filament twist is based more on cross-bridge density and should be less sensitive to troponin at least within regions containing appreciable cross-bridge density.

A second alternative is that cross-bridges are conformed such that they disguise the normal twist of the thin filament. The requirement for this is that the contact or bonding surfaces between actin and myosin would be differently aligned for each of the two myosin heads in the lead bridge (Taylor et al., 1989).

The third alternative hypothesizes flexibility within the actin monomer itself. The actin monomer is a two-domain structure (Kabsch et al., 1985). Some models of F actin (Egelman et al., 1983) have oriented one domain at low radius, where it establishes filament connectivity while the other domain at higher radius contributes less to filament integrity. If myosin heads bind primarily to this outer actin domain, as some recent acto-S1 reconstructions suggest (Milligan and Flicker, 1987), a flexible link between actin domains might allow deformation within the actin monomer itself to absorb some of the torsional force exerted on the thin filament by the lead bridge. This hypothesized movement between actin domains could produce the appearance of local

twist variations while preserving both uniform twist (along inner actin domains) and uniform actin–myosin contacts for both heads.

Implications for Rigor Tension Development

Can these rigor structures illuminate any features of the molecular changes that occur during muscle contraction? Rigorization produces tension and rigor fibers sustain this tension for many hours (White, 1970; Kuhn, 1978). Over a period of 1 min to 20 h the pattern and shape of rigor bridges show no obvious time dependent structural changes which might indicate that an annealing process is altering cross-bridge shape and distribution. Moreover, load-dependent structural changes are not observed (Reedy et al., 1988*b*; Reedy, M. K., and W. Longley, unpublished observations). The fibers examined here were rigorized in situ and were fixed under the tension resulting from a 3% stretch, applied in rigor to ensure excellent orientation in the x-ray beam. The prolonged maintenance of rigor tension in IFM and the lack of any obvious microscopic evidence of annealing in the cross-bridge lattice suggests that after the rigor power stroke, the myosin heads do not redistribute their thin filament attachments. Furthermore, when rigor IFM fibers are stretched 1–2% per hour, sarcomeres rupture rather than display any signs of cross-bridge slippage (Somasundaram, B., and M. K. Reedy, unpublished observations). Moreover, regardless of external load, even the smallest lattice motif, the double chevron, seems to maintain indefinitely the internal local strain expressed in the two different bridge angles. The invariance of rigor bridge pattern over time and regardless of load makes it reasonable to interpret our reconstructions as representative of the initial transformation to rigor. In this context the asynchronous cross-bridge formation of contracting muscle becomes a temporal sequence of rigor attachments. The final bimodal distribution of cross-bridge structures in rigor will depend on the interplay of lattice constraints, which determine where the myosin heads are attached, with the balance of force and resistance to filament sliding between early and late attaching cross-bridges.

The presence of rigor of two myosin head conformations, one associated with the beginning of the power stroke and the other with the end, creates a paradox; are both bridges at the end of the power stroke? Because these two rigor structures develop immediately upon rigorization and sustain tension for prolonged periods, it is reasonable to suppose that they embody the tension generating events. The angled configuration of myosin heads in acto-S1 suggests that this conformation represents the lowest energy state in the absence of ATP, and by inference the end of the cross-bridge stroke.

The presence of both 90° and 45° heads in rigor fibers can be reconciled to a rowing model of the power stroke if a temporal attachment sequence traps the stroke at different stages. Under this interpretation, heads that attach earlier and complete the power stroke may then produce enough resistance to filament sliding to prevent later attaching heads from completing the transition to 45°. There are two notable consequences of a "trapping" mechanism. First, the 90° bridges may not have finished a power stroke and would not be at the lowest energy state. Second, early attaching bridges that have completed the power stroke may be driven past their lowest energy state to a region where they are producing negative force. Since the rigor fiber is producing and sustaining tension, it follows that heads trapped at 90° may be exerting positive force. That is to say, they may be capable of producing filament sliding if the balancing negative forces could be relieved by detachment of the restraining bridges. This hypothesis implies that while rigor represents the lowest sum of energy possible for a particular arrangement of myosin heads and actin, each cross-bridge within the lattice need not be at the bottom of its energy well.

A balance between positive and negative force-bearing bridges has been hypothesized to account for the force/velocity relationship under varying loads (Huxley, 1957). In this model, negative force cross-bridges remain attached to actin after the power stroke and thereby produce a drag on filament sliding as they are displaced from their thick filament origins. This force remains until they eventually release from actin by rebinding ATP. Negative force cross-bridges have been recently demonstrated, not only in active muscle (Goldman, 1987) but also in rigor muscle (Goldman, Y., J. A. McCray, and D. P. Vallette, unpublished observations). We are inclined toward the view that some of the lead bridges are the negative force bearing bridges for the simple reason that they are the only ones that reveal an angled shape identified above as the end of the power stroke. They are thus the most likely bridges to be carried into the negative force region. This view implies that the 90° bridges bear the positive force.

Although cross-bridge detachment-reattachment equilibria are greatly slowed in rigor, one still expects "equilibrium cross-bridge" behavior (Schoenberg and Eisenberg, 1985), whereby myosin heads which exert or bear force should eventually detach and reattach at positions of lesser strain. Nevertheless, strain relief by cross-bridge redistribution seems not to proceed readily in the rigor lattice of IFM. Yet if lead and rear bridges exert opposing axial forces, what can prevent one or the other from relocating into the intradoublet gap where a single actin subunit appears unoccupied more often than not? The answer is not clear, but could be different for lead and rear bridges. At the lead bridge, internal strain distribution within two-headed bridges might render unlikely such "backward" migration, since it would require the trailing head, already strained at 90°, to relocate to an even more strained anti-rigor angle. At the rear bridge, the heavy troponin peculiar to IFM may interact directly with the myosin head (Bullard et al., 1988), which in this context may stabilize the rigor contact.

Ours is the first observation of a 90° cross-bridge in the strong binding configuration and may have significant implications for tension generation in muscle. In the foregoing discussion we have suggested that the 90° bridges are capable of generating force. The defining structural feature of these 90° rigor bridges is that they are slewed and bent around the thin filament. This slewing and bending is an expression of the multidomain structure of the myosin heads. Can this slewing and bending of the 90° bridges in rigor help to suggest a model for the structural change that accompanies tension production? Work with AMPPNP has established that nucleotide binding and coordinated tension loss are correlated with a straightening of the crossbridge in the azimuthal plane rather than any overall angle change. Specifically, when rigor fibers of IFM are saturated with AMPPNP at 23°, there is a 70% drop in tension without a coincident drop in rigor stiffness (Reedy et al., 1988*a*,*b*). Electron micrographs

of these fibers in 15-nm transverse sections show conversion from the commonly observed flared X of rigor to a straightened X with no apparent change in tilt angle of cross-bridges seen in longitudinal sections. Moreover, this 70% drop in tension can be reversed by only a 2-nm/half sarcomere reextension of the fibers (Marston et al., 1979; Tregear, 1988). These observations suggest that this tension loss involves primarily unbending and unslewing of the head within the azimuthal plane coordinated with AMPPNP binding. The reverse step, the change from straight to bent conformation accompanies nucleotide release and restores tension (Reedy et al., 1988*b*). That a large reversible loss in tension can be accounted for by only 2 nm of filament movement accompanied primarily by azimuthal changes in head shape argues that domain realignments within the head between bent and straightened conformations are a significant component of tension production. It is this conformational change from a straight to a bent shape during rigor induction that may also provide the force for untwisting the thin filament at the lead bridge.

X-ray evidence from isometrically contracting muscle has shown an increase in intensity on actin-based layer lines but little correspondence to the rigor intensity profile (Matsubara et al., 1984; Maeda et al., 1986; Wakabayashi et al., 1988). In the model we are considering, tension can be produced without a requirement for a large angle change in the head but can occur though an azimuthal realignment of domains in the myosin head coupled with release of nucleotide or its cleavage products. Cross-bridges at the 45° rigor angle would not be necessary to maintain tension in isometrically contracting muscle. Accumulation of a large number of myosin heads at 45° or triangular two-headed bridges would not occur because they may have too short a lifetime and therefore form too small a population in the muscle lattice to be detected by x-rays. The x-ray diagram in isometric contraction would instead be dominated by scattering from an accumulation of myosin heads near the 90° orientation, some in the pretension and some in the tension state. Electron microscopy has shown straightened cross-bridges at 90° in a state with high stiffness that will not bear tension (Reedy et al., 1988*b*). In our model heads bound in the 90° state would be azimuthally disordered because they would be distributed among the straight and bent conformations. We suggest that a 90° force bearing cross-bridge like that identified here in rigor may play a significant role in muscle contraction.

The authors would like to dedicate this paper to the memory of Dr. William Longley, a valued friend and colleague, whose custom microdensitometer enabled us to begin this work. We thank Ms. Vivian Fowler for typing the manuscript and Ms. Suzanne Goodman for technical assistance.

This research supported by National Institutes of Health grants GM 30598, AM 14317, and grants from the Muscular Dystrophy Association. The PDS scanner was purchased from funds supplied by National Institutes of Health grant RR02283 and National Science Foundation grant PCM 8400167. K. A. Taylor is an Established Investigator of the American Heart Association.

Received for publication 2 December 1988 and in revised form 12 May 1989.

References

Amos, L. A. 1985. Structure of muscle filaments studied by electron microscopy. *Annu. Rev. Biophys. Biophys. Chem.* 14:291–313.

Applegate, D., and P. Flicker. 1987. New states of actomyosin. *J. Biol. Chem.* 262:6856–6863.

Barnett, V. A., and D. D. Thomas. 1984. Saturation transfer EPR of spin labeled muscle fibers: dependence on sarcomere length. *J. Mol. Biol.* 179:83–102.

Bennett, P. M. 1974. Decrease in section thickness on exposure to the electron beam: the use of tilted sections in estimating the amount of shrinkage. *J. Cell Sci.* 15:693–701.

Berriman, J., and K. R. Leonard. 1986. Methods for specimen thickness determination in electron microscopy II. Changes in thickness with dose. *Ultramicroscopy.* 19:349–366.

Bullard, B., R. Dabrowska, and L. Winkelman. 1973. The contractile and regulatory proteins of insect flight muscle. *Biochem. J.* 135:277–286.

Bullard, B., K. Leonard, A. Larkins, G. Butcher, C. Karlik, and E. Fyrgerg. 1988. Troponin of asynchronous flight muscle. *J. Mol. Biol.* 204:621–637.

Cooke, R. 1981. Stress does not alter the conformation of a domain of the myosin crossbridge in rigor muscle fibers. *Nature (Lond.).* 294:570–574.

Cooke, R., M. S. Crowder, and D. D. Thomas. 1982. Orientation of spin-labels attached to cross-bridges in contracting muscle fibers. *Nature (Lond.).* 300:776–778.

Craig, R., L. E. Green, and E. Eisenberg. 1985. Structure of the actin-myosin complex in the presence of ATP. *Proc. Natl. Acad. Sci. USA.* 82:3247–3251.

Egelman, E. H., N. Francis, and D. J. DeRosier. 1982. F-actin is a helix with a random variable twist. *Nature (Lond.).* 298:131–135.

Egelman, E. H., N. Francis, and D. J. DeRosier. 1983. Helical disorder and the filament structure of F-actin are elucidated by the angle-layered aggregate. *J. Mol. Biol.* 166:605–629.

Flicker, P. F., G. N. Phillips, Jr., and C. Cohen. 1982. Troponin and its interactions with tropomyosin. An electron microscope study. *J. Mol. Biol.* 162:495–501.

Goody, R. S., and K. C. Holmes. 1983. Crossbridges and the mechanism of muscle contraction. *Biochim. Biophys. Acta.* 726:13–39.

Green, L. E., and E. Eisenberg. 1980. The binding of heavy meromyosin to F-actin. *J. Biol. Chem.* 255:549–554.

Goldman, Y. E. 1987. Measurement of sarcomere shortening in skinned fibers from frog muscle by white light diffraction. *Biophys. J.* 52:57–68.

Haselgrove, J. C. 1970. X-ray diffraction studies on muscle. Ph.D. thesis. University of Cambridge.

Haselgrove, J. C., and M. K. Reedy. 1978. Modelling rigor cross-bridge patterns in muscle. I. Initial studies of the rigor lattice of insect flight muscle. *Biophys. J.* 24:713–728.

Heuser, J. E. 1987. Crossbridges in insect flight muscles of the blowfly (*Sarcophaga bullata*). *J. Muscle Res. Cell Motil.* 8:303–321.

Holmes, K. C., R. T. Tregear, and J. Barrington-Leigh. 1980. Interpretation of the low angle x-ray diffraction from insect fight muscle in rigor. *Proc. R. Soc. Lond. Biol. Sci.* 207:13–33.

Holser, W. T. 1958. Point groups and plane groups in a two-sided plane and their subgroups. *Z. F. Kristallogr.* 110:266–281.

Huxley, A. F. 1957. Muscle structure and theories of contraction. *Prog. Biophys. Chem.* 7:255–318.

Huxley, H. E. 1963. Electron microscope studies on the structure of natural and synthetic protein filaments from striated muscle. *J. Mol. Biol.* 7:281–308.

Huxley, H. E. 1969. The mechanism of muscular contraction. *Science (Wash. DC).* 164:1356–1366.

Kabsch, W., H. G. Mannherz, and D. Suck. 1985. Three dimensional structure of the complex of actin and DNase I at 4.5Å resolution. *EMBO (Eur. Mol. Biol. Organ.) J.* 4:2113–2118.

Kajiyama, H. 1988. Shape of the myosin head in the rigor complex. *J. Mol. Biol.* 204:639–652.

Kuhn, H. J. 1978. Cross bridge slippage induced by the ATP analogue AMP-PNP and stretch in glycerol-extracted fibrillar muscle fibres. *Biophys. Struct. Mech.* 4:159–168.

Lehman, W., B. Bullard, and K. Hammond. 1974. Calcium-dependent myosin from insect flight muscles. *J. Gen. Physiol.* 63:553–563.

Maeda, Y., C. Boulin, A. Gabriel, I. Sumner, and M. H. J. Koch. 1986. Intensity increases of actin layer-lines on activation of the *Limulus* muscle. *Biophys. J.* 50:1035–1042.

Marston, S. B., R. T. Tregear, C. D. Rodger, and M. L. Clarke. 1979. Coupling between the enzymatic site of myosin and the mechanical output of muscle. *J. Mol. Biol.* 128:111–126.

Matsubara, I., N. Yagi, H. Miura, M. Ozeki, and T. Izumi. 1984. Intensification of the 5.9-nm actin layer line in contracting muscle. *Nature (Lond.).* 312:471–473.

Miller, A., and R. T. Tregear. 1972. The structure of insect fibrillar flight muscle in the presence and absence of ATP. *J. Mol. Biol.* 70:85–104.

Milligan, R. A., and P. F. Flicker. 1987. Structural relationships of actin, myosin, and tropomyosin revealed by cryo-electron microscopy. *J. Cell Biol.* 105:29–39.

Moore, P. B., H. E. Huxley, and D. J. DeRosier. 1970. Three dimensional reconstruction of F-actin, thin filaments and decorated thin filaments. *J. Mol. Biol.* 50:279–295.

Naylor, G. R. S., and R. J. Podolsky. 1981. X-ray diffraction of strained muscle fibers in rigor. *Proc. Natl. Acad. Sci. USA.* 78:5559–5563.

Reedy, M. K., K. C. Holmes, and R. T. Tregear. 1965. Induced changes in

orientation of the cross-bridges of glycerinated insect flight muscle. *Nature (Lond.).* 207:1276–1280.

Reedy, M. K. 1968. Ultrastructure of insect flight muscle. I. Screw sense and structural grouping in the rigor cross-bridge lattice. *J. Mol. Biol.* 31:155–176.

Reedy, M. K., and M. C. Reedy. 1985. Rigor crossbridge structure in tilted single filament layers and flared-X formations from insect flight muscle. *J. Mol. Biol.* 185:145–176.

Reedy, M. C., M. K. Reedy, and R. T. Tregear. 1988*a*. Two attached non-rigor crossbridge forms. *In* Molecular Mechanism of Muscle Contraction. H. Sugi and G. H. Pollack, editors. Plenum Publishing Corp., New York. 5–11.

Reedy, M. C., M. K. Reedy, and R. T. Tregear. 1988*b*. Two attached non-rigor crossbridge forms in insect flight muscle. *J. Mol. Biol.* 204:357–383.

Rodger, C. D., and R. T. Tregear. 1974. Crossbridge angle when ADP is bound to myosin. *J. Mol. Biol.* 86:495–497.

Schoenberg, M., and E. Eisenberg. 1985. Muscle cross-bridge kinetics in rigor and in the presence of ATP analogues. *Biophys. J.* 48:863–871.

Stokes, D. L., and D. J. DeRosier. 1987. The variable twist of actin and its modulation by actin-binding proteins. *J. Cell Biol.* 104:1005–1017.

Taylor, K. A., and L. A. Amos. 1981. A new model for the geometry of the binding of myosin crossbridges to muscle thin filaments. *J. Mol. Biol.* 147:297–324.

Taylor, K., L. Dux, and A. Martonosi. 1984*a*. Structure of the vanadate induced crystals of sarcoplasmic reticulum Ca^{2+}-ATPase. *J. Mol. Biol.* 174:193–204.

Taylor, K. A., M. C. Reedy, L. Córdova and M. K. Reedy. 1984*b*. Three-dimensional reconstruction of rigor insect flight muscle from tilted thin sections. *Nature (Lond.).* 310:285–291.

Taylor, K. A., M. C. Reedy, L. Córdova, and M. K. Reedy. 1986. Image reconstruction using electron micrographs of insect flight muscle: use of thick transverse sections to supplement data from tilted thin longitudinal sections. *Biophys. J.* 49:353–364.

Taylor, K. A., M. C. Reedy, L. Córdova, and M. K. Reedy. 1989. Three-dimensional image reconstruction of insect flight muscle. I. The rigor myac layer. *J. Cell Biol.* 109:1085–1102.

Thomas, D. D. 1987. Spectroscopic probes of muscle cross-bridge rotation. *Annu. Rev. Physiol.* 49:691–709.

Thomas, D. D., and R. Cooke. 1980. Orientation of spin-labelled myosin heads in glycerinated muscle fibers. *Biophys. J.* 32:891–906.

Thomas, D. D., R. Cooke, and V. A. Barnett. 1983. Orientation and rotational mobility of spin-labelled myosin heads in insect flight muscle in rigor. *J. Muscle Res. Cell Motil.* 4:376–378.

Toyoshima, C., and T. Wakabayashi. 1985. Three-dimensional image analysis of the complex of thin filaments and myosin molecules from skeletal muscle. IV. Reconstitution from minimal- and high-dose images of the actin-tropomyosin-myosin subfragment-1 complex. *J. Biochem.* 97:219–243.

Tregear, R. T. 1988. Mechanical properties of demembranated muscle fibres in the presence of MgAMPPNP. *In* Molecular Mechanism of Muscle Contraction. H. Sugi and G. H. Pollack, editors. Plenum Publishing Corp., New York. 513–526.

Trombitas, K., P. H. Baatsen, and G. H. Pollack. 1988. Effect of tension on the rigor cross-bridge angle. *In* Molecular Mechanism of Muscle Contraction. H. Sugi and G. H. Pollack, editors. Plenum Publishing Corp., New York. 17–28.

Vibert, P., and R. Craig. 1982. Three dimensional reconstruction of thin filaments decorated with a Ca^{2+}-regulated myosin. *J. Mol. Biol.* 157:299–319.

Vigers, G. P. A., R. A. Crowther, and B. M. F. Pearse. 1986. Three-dimensional structure of clathrin cages in ice. *EMBO (Eur. Mol. Biol. Organ.) J.* 5:529–534.

Wakabayashi, K., Y. Ueno, Y. Amemiya, and H. Tanaka. 1988. Intensity changes of actin-based layer lines from frog skeletal muscles during an isometric contraction. *In* Molecular Mechanism of Muscle Contraction. H. Sugi and G. H. Pollack, editors. Plenum Publishing Corp. 353–366.

Walker, M., and J. Trinick. 1988. Visualization of domains in native and nucleotide-trapped myosin heads by negative staining. *J. Muscle Res. Cell Motil.* 9:359–366.

White, D. C. S. 1970. Rigor contraction and the effect of various phosphate compounds on glycerinated insect flight and vertebrate muscle. *J. Physiol.* 208:583–605.

Wray, J. S., P. J. Vibert, and C. Cohen. 1978. Actin filaments in muscle: pattern of myosin and tropomyosin-troponin attachment. *J. Mol. Biol.* 124:501–521.

Yanagida, T. 1984. Angles of fluorescently labelled myosin heads and actin monomers in contracting and rigor strained muscle fibers. *In* Contractile Mechanisms in Muscle Contraction. G. H. Pollack and H. Sugi, editors. Plenum Publishing Corp. 397–411.

Yanagida, T. 1985. Angle of active site of myosin heads in contracting muscle during sudden length changes. *J. Muscle Res. Cell Motil.* 6:43–52.